Azimuthal transverse single-spin asymmetries of inclusive jets and charged pions within jets from polarized-proton collisions at $\sqrt{s} = 500$ GeV

L. Adamczyk,[1] J. R. Adams,[29] J. K. Adkins,[19] G. Agakishiev,[17] M. M. Aggarwal,[31] Z. Ahammed,[54] N. N. Ajitanand,[42] I. Alekseev,[15,26] D. M. Anderson,[44] R. Aoyama,[48] A. Aparin,[17] D. Arkhipkin,[3] E. C. Aschenauer,[3] M. U. Ashraf,[47] A. Attri,[31] G. S. Averichev,[17] X. Bai,[7] V. Bairathi,[27] K. Barish,[50] A. Behera,[42] R. Bellwied,[46] A. Bhasin,[16] A. K. Bhati,[31] P. Bhattarai,[45] J. Bielcik,[10] J. Bielcikova,[11] L. C. Bland,[3] I. G. Bordyuzhin,[15] J. Bouchet,[18] J. D. Brandenburg,[36] A. V. Brandin,[26] D. Brown,[23] J. Bryslawskyj,[50] I. Bunzarov,[17] J. Butterworth,[36] H. Caines,[58] M. Calderón de la Barca Sánchez,[5] J. M. Campbell,[29] D. Cebra,[5] I. Chakaberia,[3] P. Chaloupka,[10] Z. Chang,[44] N. Chankova-Bunzarova,[17] A. Chatterjee,[54] S. Chattopadhyay,[54] X. Chen,[21] X. Chen,[39] J. H. Chen,[41] J. Cheng,[47] M. Cherney,[9] W. Christie,[3] G. Contin,[22] H. J. Crawford,[4] S. Das,[7] T. G. Dedovich,[17] J. Deng,[40] I. M. Deppner,[51] A. A. Derevschikov,[33] L. Didenko,[3] C. Dilks,[32] X. Dong,[22] J. L. Drachenberg,[20] J. E. Draper,[5] J. C. Dunlop,[3] L. G. Efimov,[17] N. Elsey,[56] J. Engelage,[4] G. Eppley,[36] R. Esha,[6] S. Esumi,[48] O. Evdokimov,[8] J. Ewigleben,[23] O. Eyser,[3] R. Fatemi,[19] S. Fazio,[3] P. Federic,[11] P. Federicova,[10] J. Fedorisin,[17] Z. Feng,[7] P. Filip,[17] E. Finch,[49] Y. Fisyak,[3] C. E. Flores,[5] J. Fujita,[9] L. Fulek,[1] C. A. Gagliardi,[44] F. Geurts,[36] A. Gibson,[53] M. Girard,[55] D. Grosnick,[53] D. S. Gunarathne,[43] Y. Guo,[18] A. Gupta,[16] W. Guryn,[3] A. I. Hamad,[18] A. Hamed,[44] A. Harlenderova,[10] J. W. Harris,[58] L. He,[34] S. Heppelmann,[32] S. Heppelmann,[5] N. Herrmann,[51] A. Hirsch,[34] S. Horvat,[58] B. Huang,[8] T. Huang,[28] X. Huang,[47] H. Z. Huang,[6] T. J. Humanic,[29] P. Huo,[42] G. Igo,[6] W. W. Jacobs,[14] A. Jentsch,[45] J. Jia,[3,42] K. Jiang,[39] S. Jowzaee,[56] E. G. Judd,[4] S. Kabana,[18] D. Kalinkin,[14] K. Kang,[47] D. Kapukchyan,[50] K. Kauder,[56] H. W. Ke,[3] D. Keane,[18] A. Kechechyan,[17] Z. Khan,[8] D. P. Kikoła,[55] C. Kim,[50] I. Kisel,[12] A. Kisiel,[55] L. Kochenda,[26] M. Kocmanek,[11] T. Kollegger,[12] L. K. Kosarzewski,[55] A. F. Kraishan,[43] L. Krauth,[50] P. Kravtsov,[26] K. Krueger,[2] N. Kulathunga,[46] L. Kumar,[31] J. Kvapil,[10] J. H. Kwasizur,[14] R. Lacey,[42] J. M. Landgraf,[3] K. D. Landry,[6] J. Lauret,[3] A. Lebedev,[3] R. Lednicky,[17] J. H. Lee,[3] X. Li,[39] W. Li,[41] Y. Li,[47] C. Li,[39] J. Lidrych,[10] T. Lin,[14] M. A. Lisa,[29] F. Liu,[7] P. Liu,[42] Y. Liu,[44] H. Liu,[14] T. Ljubicic,[3] W. J. Llope,[56] M. Lomnitz,[22] R. S. Longacre,[3] X. Luo,[7] S. Luo,[8] G. L. Ma,[41] L. Ma,[41] R. Ma,[3] Y. G. Ma,[41] N. Magdy,[42] R. Majka,[58] D. Mallick,[27] S. Margetis,[18] C. Markert,[45] H. S. Matis,[22] D. Mayes,[50] K. Meehan,[5] J. C. Mei,[40] Z. W. Miller,[8] N. G. Minaev,[33] S. Mioduszewski,[44] D. Mishra,[27] S. Mizuno,[22] B. Mohanty,[27] M. M. Mondal,[13] D. A. Morozov,[33] M. K. Mustafa,[22] Md. Nasim,[6] T. K. Nayak,[54] J. M. Nelson,[4] D. B. Nemes,[58] M. Nie,[41] G. Nigmatkulov,[26] T. Niida,[56] L. V. Nogach,[33] T. Nonaka,[48] S. B. Nurushev,[33] G. Odyniec,[22] A. Ogawa,[3] K. Oh,[35] V. A. Okorokov,[26] D. Olvitt, Jr.,[43] B. S. Page,[3] R. Pak,[3] Y. Pandit,[8] Y. Panebratsev,[17] B. Pawlik,[30] H. Pei,[7] C. Perkins,[4] J. Pluta,[55] K. Poniatowska,[55] J. Porter,[22] M. Posik,[43] N. K. Pruthi,[31] M. Przybycien,[1] J. Putschke,[56] A. Quintero,[43] S. Ramachandran,[19] R. L. Ray,[45] R. Reed,[23] M. J. Rehbein,[9] H. G. Ritter,[22] J. B. Roberts,[36] O. V. Rogachevskiy,[17] J. L. Romero,[5] J. D. Roth,[9] L. Ruan,[3] J. Rusnak,[11] O. Rusnakova,[10] N. R. Sahoo,[44] P. K. Sahu,[13] S. Salur,[37] J. Sandweiss,[58] M. Saur,[11] J. Schambach,[45] A. M. Schmah,[22] W. B. Schmidke,[3] N. Schmitz,[24] B. R. Schweid,[42] J. Seger,[9] M. Sergeeva,[6] R. Seto,[50] P. Seyboth,[24] N. Shah,[41] E. Shahaliev,[17] P. V. Shanmuganathan,[23] M. Shao,[39] W. Q. Shen,[41] S. S. Shi,[7] Z. Shi,[22] Q. Y. Shou,[41] E. P. Sichtermann,[22] R. Sikora,[1] M. Simko,[11] S. Singha,[18] M. J. Skoby,[14] N. Smirnov,[58] D. Smirnov,[3] W. Solyst,[14] P. Sorensen,[3] H. M. Spinka,[2] B. Srivastava,[34] T. D. S. Stanislaus,[53] D. J. Stewart,[58] M. Strikhanov,[26] B. Stringfellow,[34] A. A. P. Suaide,[38] T. Sugiura,[48] M. Sumbera,[11] B. Summa,[32] Y. Sun,[39] X. Sun,[7] X. M. Sun,[7] B. Surrow,[43] D. N. Svirida,[15] A. H. Tang,[3] Z. Tang,[39] A. Taranenko,[26] T. Tarnowsky,[25] A. Tawfik,[57] J. Thäder,[22] J. H. Thomas,[22] A. R. Timmins,[46] D. Tlusty,[36] T. Todoroki,[3] M. Tokarev,[17] S. Trentalange,[6] R. E. Tribble,[44] P. Tribedy,[3] S. K. Tripathy,[13] B. A. Trzeciak,[10] O. D. Tsai,[6] T. Ullrich,[3] D. G. Underwood,[2] I. Upsal,[29] G. Van Buren,[3] G. van Nieuwenhuizen,[3] A. N. Vasiliev,[33] F. Videbæk,[3] S. Vokal,[17] S. A. Voloshin,[56] A. Vossen,[14] G. Wang,[6] Y. Wang,[7] F. Wang,[34] Y. Wang,[47] G. Webb,[3] J. C. Webb,[3] L. Wen,[6] G. D. Westfall,[25] H. Wieman,[22] S. W. Wissink,[14] R. Witt,[52] Y. Wu,[18] Z. G. Xiao,[47] G. Xie,[39] W. Xie,[34] Y. F. Xu,[41] J. Xu,[7] Q. H. Xu,[40] N. Xu,[22] Z. Xu,[3] S. Yang,[3] Y. Yang,[28] C. Yang,[40] Q. Yang,[40] Z. Ye,[8] Z. Ye,[8] L. Yi,[58] K. Yip,[3] I.-K. Yoo,[35] N. Yu,[7] H. Zbroszczyk,[55] W. Zha,[39] Z. Zhang,[41] J. Zhang,[21] S. Zhang,[39] S. Zhang,[41] J. Zhang,[22] Y. Zhang,[39] X. P. Zhang,[47] J. B. Zhang,[7] J. Zhao,[34] C. Zhong,[41] L. Zhou,[39] C. Zhou,[41] X. Zhu,[47] Z. Zhu,[40] and M. Zyzak[12]

(STAR Collaboration)

[1]*AGH University of Science and Technology, FPACS, Cracow 30-059, Poland*
[2]*Argonne National Laboratory, Argonne, Illinois 60439*
[3]*Brookhaven National Laboratory, Upton, New York 11973*
[4]*University of California, Berkeley, California 94720*
[5]*University of California, Davis, California 95616*
[6]*University of California, Los Angeles, California 90095*

[7]*Central China Normal University, Wuhan, Hubei 430079*
[8]*University of Illinois at Chicago, Chicago, Illinois 60607*
[9]*Creighton University, Omaha, Nebraska 68178*
[10]*Czech Technical University in Prague, FNSPE, Prague, 115 19, Czech Republic*
[11]*Nuclear Physics Institute AS CR, 250 68 Prague, Czech Republic*
[12]*Frankfurt Institute for Advanced Studies FIAS, Frankfurt 60438, Germany*
[13]*Institute of Physics, Bhubaneswar 751005, India*
[14]*Indiana University, Bloomington, Indiana 47408*
[15]*Alikhanov Institute for Theoretical and Experimental Physics, Moscow 117218, Russia*
[16]*University of Jammu, Jammu 180001, India*
[17]*Joint Institute for Nuclear Research, Dubna, 141 980, Russia*
[18]*Kent State University, Kent, Ohio 44242*
[19]*University of Kentucky, Lexington, Kentucky 40506-0055*
[20]*Lamar University, Physics Department, Beaumont, Texas 77710*
[21]*Institute of Modern Physics, Chinese Academy of Sciences, Lanzhou, Gansu 730000*
[22]*Lawrence Berkeley National Laboratory, Berkeley, California 94720*
[23]*Lehigh University, Bethlehem, Pennsylvania 18015*
[24]*Max-Planck-Institut fur Physik, Munich 80805, Germany*
[25]*Michigan State University, East Lansing, Michigan 48824*
[26]*National Research Nuclear University MEPhI, Moscow 115409, Russia*
[27]*National Institute of Science Education and Research, HBNI, Jatni 752050, India*
[28]*National Cheng Kung University, Tainan 70101*
[29]*Ohio State University, Columbus, Ohio 43210*
[30]*Institute of Nuclear Physics PAN, Cracow 31-342, Poland*
[31]*Panjab University, Chandigarh 160014, India*
[32]*Pennsylvania State University, University Park, Pennsylvania 16802*
[33]*Institute of High Energy Physics, Protvino 142281, Russia*
[34]*Purdue University, West Lafayette, Indiana 47907*
[35]*Pusan National University, Pusan 46241, Korea*
[36]*Rice University, Houston, Texas 77251*
[37]*Rutgers University, Piscataway, New Jersey 08854*
[38]*Universidade de Sao Paulo, Sao Paulo, Brazil, 05314-970*
[39]*University of Science and Technology of China, Hefei, Anhui 230026*
[40]*Shandong University, Jinan, Shandong 250100*
[41]*Shanghai Institute of Applied Physics, Chinese Academy of Sciences, Shanghai 201800*
[42]*State University of New York, Stony Brook, New York 11794*
[43]*Temple University, Philadelphia, Pennsylvania 19122*
[44]*Texas A&M University, College Station, Texas 77843*
[45]*University of Texas, Austin, Texas 78712*
[46]*University of Houston, Houston, Texas 77204*
[47]*Tsinghua University, Beijing 100084*
[48]*University of Tsukuba, Tsukuba, Ibaraki, Japan, 305-8571*
[49]*Southern Connecticut State University, New Haven, Connecticut 06515*
[50]*University of California, Riverside, California 92521*
[51]*University of Heidelberg, Heidelberg, Baden-Württemberg, Germany*
[52]*United States Naval Academy, Annapolis, Maryland 21402*
[53]*Valparaiso University, Valparaiso, Indiana 46383*
[54]*Variable Energy Cyclotron Centre, Kolkata 700064, India*
[55]*Warsaw University of Technology, Warsaw 00-661, Poland*
[56]*Wayne State University, Detroit, Michigan 48201*
[57]*World Laboratory for Cosmology and Particle Physics (WLCAPP), Cairo 11571, Egypt*
[58]*Yale University, New Haven, Connecticut 06520*

(Received 23 August 2017; published 2 February 2018)

We report the first measurements of transverse single-spin asymmetries for inclusive jet and jet + $\pi^{\pm}$ production at midrapidity from transversely polarized proton-proton collisions at $\sqrt{s} = 500$ GeV. The data were collected in 2011 with the STAR detector sampled from 23 pb^{-1} integrated luminosity with an average beam polarization of 53%. Asymmetries are reported for jets with transverse momenta $6 < p_T < 55$ GeV/c and pseudorapidity $|\eta| < 1$. Presented are measurements of the inclusive-jet azimuthal transverse single-spin asymmetry, sensitive to twist-3 initial-state quark-gluon correlators; the Collins asymmetry, sensitive to quark transversity coupled to the polarized Collins fragmentation function; and the first measurement of the "Collins-like" asymmetry, sensitive to linearly polarized gluons. Within the present statistical precision, inclusive-jet and Collins-like asymmetries are small, with the latter allowing the first experimental constraints on gluon linear polarization in a polarized proton. At higher values of jet transverse momenta, we observe the first nonzero Collins asymmetries in polarized-proton collisions, with a statistical significance of greater than 5σ. The results span a range of x similar to results from semi-inclusive deep-inelastic scattering but at much higher Q^2. The Collins results enable tests of universality and factorization breaking in the transverse momentum-dependent formulation of perturbative quantum chromodynamics.

DOI: 10.1103/PhysRevD.97.032004

I. INTRODUCTION

The partonic structure of the nucleon at leading twist in a collinear picture can be described by three parton distribution functions (PDFs): the unpolarized parton distribution, $f(x, Q^2)$; the parton helicity distribution, $\Delta f(x, Q^2)$; and the transversity distribution, $h_1(x, Q^2)$ [1]. Here, x denotes the parton light-cone momentum fraction, while Q^2 denotes the momentum transfer. The unpolarized PDFs are constrained over a large range of x and Q^2 by unpolarized lepton-proton experiments at HERA (e.g. Ref. [2] and references therein). Helicity distribution constraints have required observables from the interaction of spin-polarized probes. Recent global analyses have combined data from polarized deep-inelastic scattering (DIS), semi-inclusive DIS (SIDIS), and proton-proton experiments to extract helicity distributions for quarks, antiquarks, and gluons [3–6]. Of the three leading-twist PDFs, transversity, which describes the transverse polarization of quarks inside a transversely polarized nucleon, has proven the most difficult to probe. This is due to its chiral-odd nature that requires transversity to couple to another chiral-odd quantity in order to be observed.

Advances in understanding transversity have been made through the study of transverse single-spin asymmetries. In contrast to expectations based upon collinear perturbative quantum chromodynamics (pQCD) at leading twist [7], transverse single-spin asymmetries for inclusive hadron production at forward pseudorapidity from polarized-proton collisions have long been observed to be sizable, with asymmetries of a few percent persisting to transverse momentum (p_T) values as high as several GeV/c [8–14]. Moreover, the size of the asymmetries appears to be independent of center-of-mass energy, across a range of over an order of magnitude. Though the underlying mechanism driving these effects remains something of a mystery, the presence of sizable transverse single-spin asymmetries has provided an opportunity to enhance understanding of pQCD beyond the limits of collinearity and leading twist.

Nonzero transverse single-spin asymmetries can be generated in pQCD through the twist-3 and transverse-momentum-dependent (TMD) formalisms. The twist-3 formalism [15–18] utilizes initial-state and final-state multiparton correlators within the framework of collinear pQCD. Its application requires a single large-momentum scale parameter and hence is well suited for high-p_T observables such as high-energy jet and inclusive hadron production. The TMD formalism [19,20] utilizes the leading-twist framework of pQCD beyond the collinear approximation, requiring correlations between spin polarization and intrinsic transverse momentum. For example, the Sivers mechanism [19] requires a correlation between the nucleon spin polarization and the intrinsic transverse momentum, k_T, of the parton within the nucleon, while the Collins mechanism [20] requires a correlation between the polarization of a scattered quark and the momentum of a hadron fragment transverse to the scattered quark direction. The Sivers mechanism vanishes in the absence of parton orbital angular momentum [21], and the Collins mechanism is enabled by nonzero transversity coupled to the polarization-dependent "Collins" fragmentation function [20].

Unlike twist-3, the TMD approach requires two momentum scales: a large scale such as Q to enable the use of pQCD, and a soft scale such as $p_T \ll Q$ to enable sensitivity to transverse parton motion. Moreover, while TMD factorization has been proven for SIDIS as well as for Drell-Yan and weak-boson production in polarized-proton collisions [22–26], it is expected that TMD factorization may generally be broken for hadronic interactions [27,28]. The size of any such factorization breaking is not known. It has recently been argued that the cross section for

hadrons within jets produced from proton-proton collisions does factorize and only depends upon universal TMD fragmentation functions, decoupled from TMD PDFs [29]. It has also been shown that as the value of the soft TMD scale becomes larger, the twist-3 and TMD approaches are mutually consistent [30]. Furthermore, the twist-3 correlation functions are related to the k_T-integrated TMD distribution and fragmentation functions. For example, the k_T-integrated Sivers PDF [19] is related to the Efremov-Teryaev-Qiu-Sterman (ETQS) twist-3 function [15,16] and similar relations exist between the Collins and twist-3 fragmentation functions (e.g. Refs. [18,23,31]). Consequently, measurements of twist-3 and TMD observables provide an important opportunity to test formulations of QCD beyond collinearity and leading twist.

Over the past decade, SIDIS experiments have provided the first measurements of TMD observables [32–35]. These, combined with independent measurements of the Collins fragmentation function by e^+e^- experiments [36,37], have enabled the first extractions of the transversity PDF [38–42]. The kinematic limitations of the current data sets leave the transversity extractions relatively imprecise for $x \gtrsim 0.3$.

An incisive way to enhance understanding of nucleon transverse polarization structure is through the study of transverse single-spin asymmetries in the production of jets and pions within jets from polarized-proton collisions [43–45]. The p_T of the jet and pion momentum transverse to the jet axis provide the hard and soft scales, respectively, necessary for TMD factorization. By studying different modulations of the transverse single-spin asymmetry

$$A_{UT}^{\sin(\phi)} \sin(\phi) = \frac{\sigma^{\uparrow}(\phi) - \sigma^{\downarrow}(\phi)}{\sigma^{\uparrow}(\phi) + \sigma^{\downarrow}(\phi)}, \tag{1}$$

one can isolate different physics mechanisms with sensitivity to various aspects of the nucleon transverse polarization structure, e.g. quark transversity and gluon linear polarization. Measurements with high energy polarized-proton beams will extend the kinematic reach in both x and Q^2 beyond the existing SIDIS measurements. The SIDIS cross section scales with the square of the quark charge, resulting in up quarks being weighted more than down or strange quarks, a phenomenon often referred to as u-quark dominance. Consequently a large fraction of the observed π^- yields arise from the unfavored fragmentation of u quarks. Hadroproduction eliminates u-quark dominance, thereby providing enhanced sensitivity to the minority d quarks. Furthermore, polarized-proton collisions are directly sensitive to gluonic subprocesses, enabling the study of the role of gluons in the transverse polarization structure of the nucleon. Moreover, since questions remain concerning the magnitude of potential TMD factorization breaking in hadronic interactions [27–29], data from polarized-proton collisions can provide unique and crucial experimental insight into these theoretical questions.

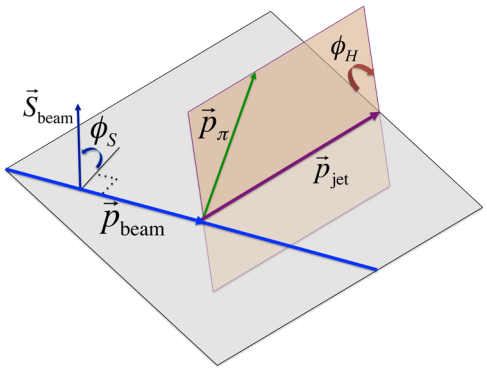

FIG. 1. Azimuthal angle definitions, following the conventions described in Ref. [43]. The direction of the beam polarization is denoted by $\vec{S}_{\text{beam}}$, while the momenta of the polarized beam, jet, and pion are, respectively, $\vec{p}_{\text{beam}}$, $\vec{p}_{\text{jet}}$, and $\vec{p}_{\pi}$.

Transverse single-spin asymmetries in the production of jets and pions within jets have a rich structure, as described in Ref. [43], the conventions of which we follow in this article. For pions within jets, the spin-dependent terms in the cross sections can be generally expressed [43]

$$\begin{aligned} &d\sigma^{\uparrow}(\phi_S,\phi_H) - d\sigma^{\downarrow}(\phi_S,\phi_H) \\ &\sim d\Delta\sigma_0 \sin(\phi_S) \\ &\quad + d\Delta\sigma_1^{-} \sin(\phi_S - \phi_H) + d\Delta\sigma_1^{+} \sin(\phi_S + \phi_H) \\ &\quad + d\Delta\sigma_2^{-} \sin(\phi_S - 2\phi_H) + d\Delta\sigma_2^{+} \sin(\phi_S + 2\phi_H), \end{aligned} \tag{2}$$

where the $d\Delta\sigma$ terms describe various combinations of distribution and fragmentation functions. Sinusoidal modulations in particle production can be measured with respect to two azimuthal angles: ϕ_S, the azimuthal angle between the proton transverse spin polarization vector and the jet scattering plane, and ϕ_H, the azimuthal angle of the pion relative to the jet scattering plane (Fig. 1). The inclusive jet asymmetry, the $\sin(\phi_S)$ modulation of A_{UT}, commonly expressed as A_N, is an observable with a single hard scale and therefore driven by the twist-3 distributions [17]. This observable is sensitive to the k_T-integrated Sivers function. The $\sin(\phi_S - \phi_H)$ modulation of A_{UT} yields sensitivity to transversity coupled to the polarized Collins fragmentation function. Through the $\sin(\phi_S - 2\phi_H)$ modulation of A_{UT}, one may gain sensitivity to gluon linear polarization coupled to the so-called "Collins-like" fragmentation function, the gluon analog of the Collins fragmentation function. While the quark-based Collins asymmetry has been measured in SIDIS, the Collins-like asymmetry has never been measured; and gluon linear polarization in the polarized proton remains completely unconstrained. The $\sin(\phi_S + \phi_H)$ and $\sin(\phi_S + 2\phi_H)$ modulations are sensitive to the TMD transversity distribution and the Boer-Mulders distribution [46] for quarks and gluons, respectively. As Ref. [43] discusses in detail, these

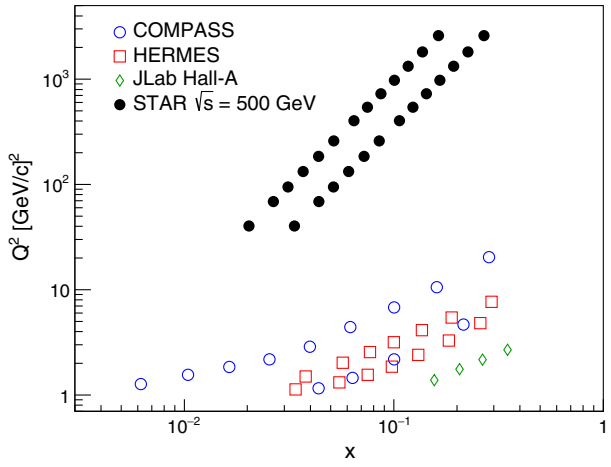

FIG. 2. Range of x and Q^2 covered by Collins asymmetry measurements from SIDIS experiments at HERMES [32,33], COMPASS [34], and Jefferson Lab Hall-A [35] in comparison to the (x, Q^2) covered by the present data as the jet p_T and η vary.

modulations are not expected to be sizable at the present kinematics, even under maximized, positivity-bound scenarios. These modulations are nevertheless measured and found to be consistent with zero. In principle, the Boer-Mulders distributions for quarks and gluons may also contribute to the $\sin(\phi_S - \phi_H)$ and $\sin(\phi_S - 2\phi_H)$ modulations. They are, however, again expected to be negligible under maximized scenarios for the present kinematics and therefore ignored.

We present the first measurements of the modulations of A_{UT} for the production of jets and pions within jets detected in the central pseudorapidity range from polarized-proton collisions at $\sqrt{s} = 500$ GeV. Included are the first measurements of the Collins-like asymmetry, sensitive to linearly polarized gluons, and the first observations of the Collins asymmetry in polarized-proton collisions. For the case of the Collins asymmetry, these measurements span ranges of x similar to those studied in SIDIS, but at substantially larger Q^2, as shown in Fig. 2. Additionally, the inclusive jet asymmetry can lend insight into twist-3 PDFs, such as the ETQS function, and, thus the Sivers function. In the lower jet-p_T range where production is dominated by gluonic subprocesses (Fig. 3), the inclusive jet measurements may yield insight into the quark-gluon and three-gluon twist-3 functions and potentially the gluon Sivers function that is largely unconstrained [47]. The present data at $\sqrt{s} = 500$ GeV provide improved sensitivity to gluonic subprocess over previous inclusive jet measurements at $\sqrt{s} = 200$ GeV [48].

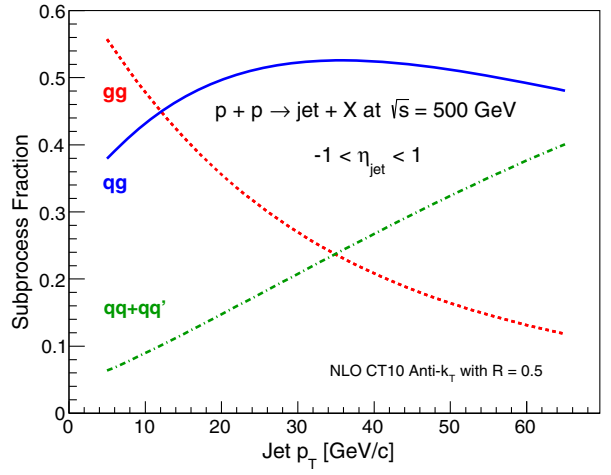

FIG. 3. Fraction of next-to-leading order (NLO) cross section [49,50] arising from quark-quark (dot-dashed line), gluon-gluon (dotted line), or quark-gluon (solid line) interactions. The fractions are shown as a function of jet p_T for jets produced within the pseudorapidity range $-1 < \eta_{\rm jet} < 1$ from collisions of an energy $\sqrt{s} = 500$ GeV. See Sec. II C for discussions of the jet definitions and reconstruction.

II. DATA ANALYSIS

A. Experiment

The data were collected during the 2011 run of the Relativistic Heavy Ion Collider (RHIC) [51] with the detectors of the Solenoidal Tracker at RHIC (STAR) [52]. In addition to its role as a heavy-ion collider, RHIC is the world's only particle accelerator capable of colliding beams of polarized protons [53]. The two independently polarized proton beams are each grouped into 120 bunches and are loaded with complex patterns of spin direction. This ensures that systematic effects from asymmetries in spin-dependent beam luminosities are minimized. RHIC is capable of colliding protons with polarizations "longitudinal" (right-handed or left-handed helicity with respect to the proton momentum) or "transverse" (vertically up or down with respect to the proton momentum). The beam polarization is measured during the run using Coulomb-nuclear interference (CNI) polarimetry [54]. The relative polarization is measured with proton-carbon polarimeters [55] that are normalized to a hydrogen-jet polarimeter [56] for the absolute scale. During the 2011 RHIC run, the average beam polarizations were measured to be 53% and 52% in the clockwise ("blue") and counterclockwise ("yellow") rotating beams, respectively, as viewed from above.

The STAR detector is designed to collect data with acceptance spanning the full azimuth and nearly five units of pseudorapidity, $-1 \lesssim \eta \lesssim 4$. The present data are generally collected within the range $|\eta| < 1$. STAR is equipped with detectors such as the zero-degree calorimeter (ZDC) [57] for local polarimetry. The ZDC covers the full azimuth for $\theta < 2$ mrad. Detectors such as the vertex position detector (VPD) [58] are used for minimum-bias triggering. The VPD covers approximately half of the solid angle for $4.2 < \eta < 5.1$. Among the subsystems utilized in jet measurements, the time projection chamber (TPC) [59]

provides charged-particle tracking over the full azimuth and $|\eta| \lesssim 1.3$. The TPC, supplemented by the time-of-flight (TOF) system [60] over the range $|\eta| \lesssim 0.9$, also provides particle identification [61]. Surrounding the TPC, the barrel electromagnetic calorimeter (BEMC) [62] provides access to electromagnetic energy over the range $|\eta| < 0.98$. This access is extended from $1.09 < \eta < 2.00$ with the end cap electromagnetic calorimeter (EEMC) [63]. The BEMC and EEMC are segmented into 4800 and 720 Pb-scintillator towers, respectively, each corresponding to ~20 radiation lengths and ~1 nuclear interaction length. The calorimeters also provide fast input for event triggering. Tracks from the TPC and hits in the calorimeter towers are also used to reconstruct collision vertices [64].

B. Event selection

All events used in the present analysis were collected from polarized proton-proton collisions at $\sqrt{s} = 500$ GeV. The events are selected from four different event triggers: a minimum bias trigger requiring a coincidence in the east and west VPDs (VPDMB) and three different levels of "jet-patch" triggers (JP0, JP1, and JP2). A jet-patch trigger requires a transverse electromagnetic energy deposit above a certain threshold—6.4, 9.0, and 13.9 GeV for JP0, JP1, and JP2, respectively—within a "patch" of area $\Delta\eta \times \Delta\phi = 1.0 \times 1.0$ in one of the calorimeters. The locations of the patches are fixed in space by the hardware. The jet-patch trigger is discussed in more detail in Ref. [48]. In the 2011 run configuration, the jet-patch trigger geometry consists of 30 patches with overlapping η ranges: $-1 < \eta < 0$, $-0.6 < \eta < 0.4$, $0 < \eta < 1$, $0.4 < \eta < 1.4$, and $1 < \eta < 2$. Because of off-line improvements to detector calibrations, in addition to the hardware trigger, jet-patch triggered events are required to pass an off-line software emulation of the trigger response. A total of 81×10^6 VPDMB events and 23 pb^{-1} of JP2 triggers pass the basic quality controls for inclusion in the analysis. The effective luminosities for the prescaled JP0 and JP1 triggers fall between these two limits.

Events are required to have a primary collision vertex determined from the TPC tracking information within a longitudinal position of $|z_{\mathrm{vtx}}| < 90$ or 30 cm of the nominal interaction point for jet-patch or VPDMB triggers, respectively. For VPDMB events, this TPC z_{vtx} is further required to agree within 6 cm with the z_{vtx} determined by the VPD timing information, which removes pileup TPC vertices.

C. Jet reconstruction

A comprehensive discussion of jet reconstruction at STAR is presented in Ref. [48] (augmented in Ref. [65]), and the present analysis follows a similar approach. Jets are reconstructed from energetic BEMC and EEMC towers and from TPC charged-particle tracks passed through the "anti-k_T" jet-finding algorithm [66] as implemented in the FastJet 3.0.6 C++ package [67] using a resolution parameter of $R = 0.5$. For inclusion in the jet reconstruction, TPC tracks must be reconstructed with more than 12 TPC fit points and with more than 51% of the possible fit points. These restrictions help to eliminate pileup tracks, aid momentum resolution, and eliminate split tracks. Furthermore, the tracks are required to match within a p_T-dependent distance-of-closest approach to the collision vertex: within 2 cm for $p_T < 0.5$ GeV/c, within 1 cm for $p_T > 1.5$ GeV/c, and with a linearly tapered cut for $0.5 < p_T < 1.5$ GeV/c. Tracks with $p_T < 0.2$ GeV/c and towers with $E_T < 0.2$ GeV are not included in jet reconstruction. Including the momenta from all charged particle tracks and energy from all calorimeter towers in jet reconstruction can lead to overestimations in jet energy due to particles that leave both a track in the TPC and energy in a calorimeter. To correct for this overestimation, the track $p_T \cdot c$ is subtracted from the E_T of the tower to which it points, not allowing the corrected E_T to be less than 0 [65].

D. Jet selection

To be selected for analysis, jets are required to have $6 < p_T < 55$ GeV/c. Furthermore, jets containing tracks with $p_{T,\mathrm{track}} > 30$ GeV/c are excluded to reduce sensitivity to uncertainties in the jet momentum resolution. To reduce sensitivity to noncollision backgrounds, such as beam-gas interactions and cosmic rays (observed as neutral energy deposits in the calorimeters), jets are required to derive at least 6% of their energy from charged particles with no less than 0.5 GeV/c in total charged-particle p_T. Owing to the asymmetric electromagnetic calorimeter coverage, jets are required to fall within an asymmetric window of pseudorapidity, $-0.7 < \eta_{\mathrm{detector}} < 0.9$, with respect to the center of the detector. Additionally, the jets are required to fall within a window of $|\eta| < 1.0$ from the reconstructed collision vertex. Jets from jet-patch triggered events are required to satisfy a geometric match to a hardware jet patch with energy deposition above the nominal triggering threshold. For the present analysis, this requirement is $|\eta_{\mathrm{jet}} - \eta_{\mathrm{patch}}| < 0.6$ and $|\phi_{\mathrm{jet}} - \phi_{\mathrm{patch}}| < 0.6$. Furthermore, jets are required to have a minimum p_T of 7.1, 9.9, or 16.3 GeV/c for JP0, JP1, and JP2 events, respectively.

E. Pion selection

Charged pions are chosen for the Collins and Collins-like analyses from jets passing the aforementioned selection criteria by requiring additional restrictions beyond those applied to all particles for inclusion in jet reconstruction. These pions are required to have $0.1 < z < 0.8$, where z is the ratio of pion momentum to jet momentum (note that this definition for z is referred to as z_h in Ref. [29]). A significant portion of pions with $z < 0.1$ in low p_T jets arises from underlying event backgrounds, while $z = 0.8$ marks the limit for sufficient statistics in this data set. For simplicity, a single range of z is selected independent of jet p_T. To ensure robust

reconstruction of the relevant azimuthal angles, pions are required to fall outside a radius of $\Delta R > 0.04$, where

$$\Delta R = \sqrt{(\eta_{\rm jet} - \eta_\pi)^2 + (\phi_{\rm jet} - \phi_\pi)^2} \tag{3}$$

relative to the jet axis. This requirement is discussed further in Sec. III E. To limit contamination to the pion sample from kaons, protons, and electrons, pions are only selected for analysis if the observed dE/dx is consistent with the expected value for pions. A parameter $n_\sigma(\pi)$ is defined as

$$n_\sigma(\pi) = \frac{1}{\sigma_{\rm exp}} \ln\left(\frac{dE/dx_{\rm obs}}{dE/dx_{\pi{\rm calc}}}\right), \tag{4}$$

where $dE/dx_{\rm obs}$ is the observed value for the event, $dE/dx_{\pi{\rm calc}}$ is the expected mean dE/dx for pions of the given momentum, and $\sigma_{\rm exp}$ is the dE/dx resolution of the TPC [61]. To ensure reliable particle identification, pions are further required to contain at least six TPC fit points with valid dE/dx information. The dE/dx values for kaons and protons overlap those of pions at momenta of 1.1 GeV/c and 1.7 GeV/c, respectively, in the STAR TPC. Thus, the $n_\sigma(\pi)$ selection window is varied depending on the reconstructed particle kinematics to optimize the sample purity. The background correction procedure and sample purity are described in Sec. III G.

F. Spin asymmetry analysis

The transverse single-spin asymmetry, defined in Eq. (1), is the amplitude of the sinusoidal ϕ dependence of the spin-dependent cross section, where ϕ represents any of the relevant azimuthal angles, e.g. for the inclusive-jet, Collins, or Collins-like effects. For extraction, the present analysis utilizes the so-called "cross-ratio" method [68] for which both acceptance and luminosity effects cancel to first order. The cross ratios, ϵ, for a given bin of ϕ can be formed by combining yields from azimuthally opposite detector halves (α vs β) when the spin orientations are flipped,

$$\epsilon = \frac{\sqrt{N^\uparrow_{1,\alpha} N^\downarrow_{1,\beta}} - \sqrt{N^\downarrow_{1,\alpha} N^\uparrow_{1,\beta}}}{\sqrt{N^\uparrow_{2,\alpha} N^\downarrow_{2,\beta}} + \sqrt{N^\downarrow_{2,\alpha} N^\uparrow_{2,\beta}}}, \tag{5}$$

where N_1 is the particle yield for a given spin state in each detector half, weighted by the beam polarization for the event. N_2 is the same, though weighted by the square of the polarization. For each RHIC fill, an initial polarization (P_0), initial time (t_0), and decay slope (dP/dt) for each beam are provided by the CNI polarimeter [54]. The event-by-event polarizations are calculated as $P_0 + (dP/dt) \times \Delta t$, where Δt is the difference between t_0 and the event time stamp. An overall systematic uncertainty of $\sigma(P)/P = 3.5\%$ is assigned to both blue and yellow beams [54] and is considered an uncertainty in the vertical scale of the asymmetries.

For the present analysis, events are designated α or β for jets in the "top" ($0 < \phi_{\rm jet} < \pi$) or "bottom" ($-\pi < \phi_{\rm jet} < 0$) half of the TPC, respectively. The cross ratios are formed as functions of the azimuthal angles, and the raw asymmetries are extracted using fits of the form

$$\epsilon(\phi) = a + b \sin(\phi). \tag{6}$$

The parameter b is the raw asymmetry, while the a term is expected to be zero. It is left in the fit as a cross-check for hidden systematic effects and found to be consistent with zero in all cases. Further statistical checks are the examination of the fit χ^2 and asymmetry residual distributions. The fits are initially performed separately for each RHIC fill, event trigger, and RHIC beam. χ^2 distributions for the asymmetry extractions are evaluated by fitting with a χ^2 function allowing the parameter for the number of degrees of freedom, ν, to float. In all cases, the fits to the χ^2 distributions return values of ν consistent with the expectation from the relevant number of azimuthal angle bins and fit constraints. The weighted averages of the asymmetries are formed and the residual distributions are examined for signs of outliers or underestimated uncertainties. In each case, the residuals follow the expected form of a Gaussian with unit width centered at zero, suggesting the individual fits scatter statistically about the mean with well estimated uncertainties. For the final extractions, yields from all of the fills and the blue and yellow beams are combined to maximize the statistical precision. To allow for trigger-dependent corrections, the asymmetries are extracted trigger-by-trigger; and the corrected asymmetries are combined in a weighted average over the event trigger classes.

III. SYSTEMATIC CORRECTIONS AND UNCERTAINTIES

A. Simulations

To evaluate systematic effects such as shifts in the jet or particle kinematics or trigger and reconstruction bias, QCD events are produced with the PYTHIA Monte Carlo generator [69], they are fed through a simulated detector response, and their resulting analog-to-digital converter counts are embedded into real events, triggered randomly (zero-bias) during a nominal crossing of proton bunches. This "embedding" procedure enables accounting of such effects as out-of-time pileup that are otherwise difficult to simulate. The Monte Carlo events are generated with PYTHIA 6.426 [69] using the Perugia 0 tune [70]. In order to achieve an optimal reproduction of the calculated next-to-leading order (NLO) inclusive jet transverse momentum spectrum, the intrinsic partonic k_T parameter is set to 1 GeV/c. The detector response is emulated with the GSTAR package based upon GEANT 3.21/08 [71]. The

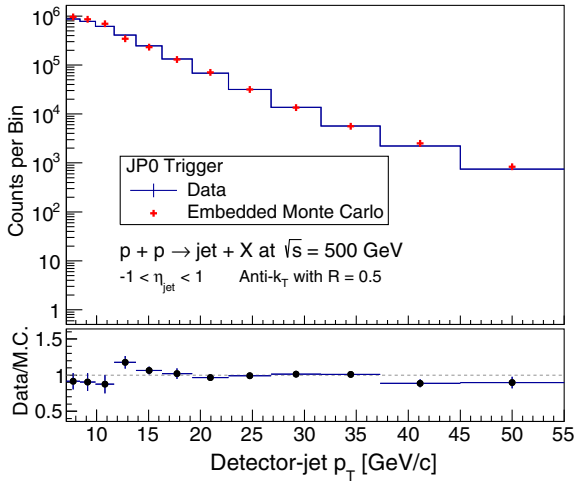

FIG. 4. Comparison of data to embedded Monte Carlo simulations for data and simulated events that satisfy the JP0 trigger. The embedding Monte Carlo distribution is normalized to match the number of data counts across the range $16.3 < p_T < 45.0\,\mathrm{GeV}/c$.

individual data-taking runs into which the PYTHIA events are embedded are chosen so as to sample the full range of luminosities encountered during the 2011 RHIC run. The runs were selected to cover a broad span of time, so that changes in detector hardware states would be well represented in the simulation sample.

The same analysis software and jet-finding algorithms applied to the data are utilized to reconstruct jets from the embedded Monte Carlo. The jet finding is applied on three levels: At the "detector-jet" level, jets are formed from TPC tracks and calorimeter towers after full simulation of the detector response. Detector jets allow direct contact between the data and simulation and exhibit excellent agreement (e.g. Fig. 4). PYTHIA "particle jets" are constructed by applying the anti-k_T algorithm with $R = 0.5$ to all stable, hadronized, final-state particles from the simulated collision, prior to detector simulation. PYTHIA "parton jets" are constructed by applying the anti-k_T algorithm with $R = 0.5$ to hard-scattered partons including initial-state and final-state radiation but excluding beam remnant and underlying event contributions.

B. Corrections to jet and pion kinematics

Detector jet and pion kinematics are corrected to the PYTHIA particle-jet level. Detector jets are associated in (η, ϕ) with both a particle jet and a parton jet in the event with the association defined as $\sqrt{\Delta\eta^2 + \Delta\phi^2} < 0.5$. Similarly, pions from associated detector jets are further associated with particles at the PYTHIA particle-jet level. Asymmetries are presented at the mean corrected kinematic values for each detector-jet level bin, determined by the kinematics of the associated PYTHIA jet. A summary of the corrected values of pion z, jet p_T, and pion j_T (pion momentum transverse to the jet axis) is presented in Fig. 5.

Uncertainties in the corrections for jet p_T and z are the quadrature combinations of statistical and systematic contributions, including those due to Monte Carlo statistics, calorimeter gains, calorimeter response to charged particles, TPC tracking efficiency, track momentum resolution, and trigger emulation. Uncertainties in the corrections for pion j_T exclude those of the jet energy scale.

C. Parton-jet associations

At lower values of jet p_T, a non-negligible probability exists that a reconstructed jet arose not from the

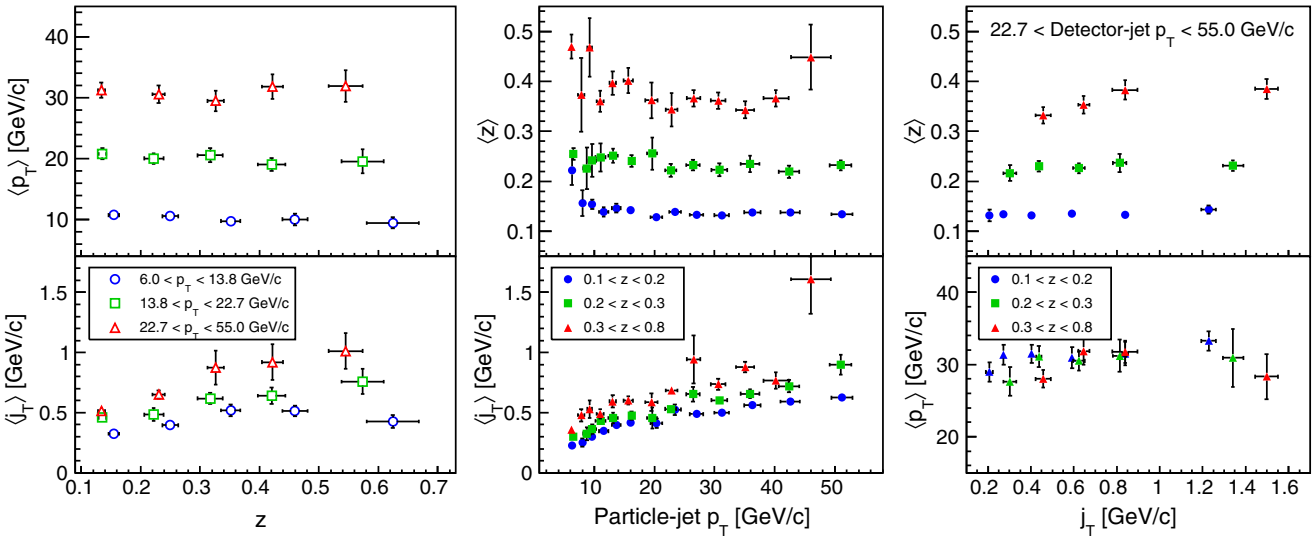

FIG. 5. Mean corrected pion z, jet p_T, and pion j_T as a function of each kinematic variable for pions within jets. Reconstructed kinematic variables are corrected to their underlying values at the PYTHIA particle-jet level. Uncertainties are the quadrature combinations of statistical and systematic contributions.

hard-scattering process but either from the underlying event or from pileup backgrounds. These probabilities are estimated by analyzing jets reconstructed from the embedded Monte Carlo events. First, an association is required between the reconstructed and generated event vertices. Association probabilities range from ∼90% to 95% at the lowest values of jet p_T to unity for $p_T > 10$ GeV/c. An association is further required between the reconstructed detector jet and a PYTHIA particle jet. These association probabilities range from ∼95% at the lowest p_T values, rising to unity by ∼10 GeV/c. Finally, an association is required between the reconstructed jet and a PYTHIA parton jet. For jets with $p_T > 10$ GeV/c, parton-jet association probabilities are near unity. Below 10 GeV/c, these association probabilities decrease steadily to ∼75% at 6 GeV/c. For purposes of the association, the matched parton or particle jets are required to have at least 1.5 GeV/c of transverse momenta.

For the asymmetries studied in the present analysis, the pertinent physics mechanisms are largely parton-level effects. For asymmetries of pions within jets, hadronization also plays a critical role. It is unclear what effects may be induced by the presence of jets from the underlying event and beam remnant; thus, the present analysis does not correct for the association probabilities. Instead, a systematic uncertainty is applied which considers the full difference between the measured asymmetry and the value if a dilution correction had been applied.

D. Trigger bias

For a given jet p_T, in particular at low p_T, the fixed size of the jet patches leads to a higher trigger efficiency for quark jets than less-collimated gluon jets (see the discussions in Refs. [48,65]). For the inclusive jet and Collins-like asymmetries, each of which are largely driven by gluonic effects, the trigger bias will suppress the asymmetries. For the Collins asymmetry, the bias should serve to enhance the effect.

The trigger bias effects are estimated with Monte Carlo simulations by comparing fractions of quark and gluon jets in triggered and unbiased event samples. In the embedded Monte Carlo, detector jets are matched to hard-scattered partons and sorted into quark and gluon jets. The unbiased jet sample, free of trigger, pileup, and reconstruction effects, is constructed from all particle jets that fall within the nominal p_T and η kinematic ranges. The trigger-bias estimates are summarized in Table I. The associated systematic uncertainties are calculated by scaling the measured asymmetry by the bias fractions from Table I and are correlated across the full range of jet p_T.

In addition to the bias in the partonic subprocess fraction, the active range of x will be somewhat distorted by the effects of reconstruction and trigger bias. To estimate these effects, the embedding simulations are analyzed, again, using the jets matched to the hard-scattered partons. The hard-scattered parton is further required to match the flavor of one of the two partons that initiated the hard-scattering process. Events are separated based on trigger, jet p_T, parton species, and η calculated relative to the incident parton direction. The effect of the bias is demonstrated in Fig. 6, where the triggered and reconstructed embedded jets are compared to those with trigger, reconstruction, and detector effects removed. Results for two cases, x_G for low-p_T VPDMB and x_Q for high-p_T JP2, are shown in Fig. 6. The VPDMB distribution agrees quite well with the unbiased distribution, while the JP2 distribution is shifted slightly to higher x, relative to the unbiased distribution. These deviations can arise from biases in both reconstruction and event triggering. Uncertainties reflected in Fig. 6 are from Monte Carlo statistics.

TABLE I. Trigger bias systematics for quark and gluonic subprocesses. The values reflect the relative difference in the fraction of quark or gluon jets between triggered and unbiased Monte Carlo events. The quark biases apply to the Collins asymmetries while the gluon biases apply to the inclusive-jet and Collins-like asymmetries. The systematics are correlated across the full range of jet p_T.

p_T Range [GeV/c]	Quark bias	Gluon bias
6.0–13.8	+17%	−10%
13.8–22.7	+8%	−6%
22.7–55.0	+3%	−3%

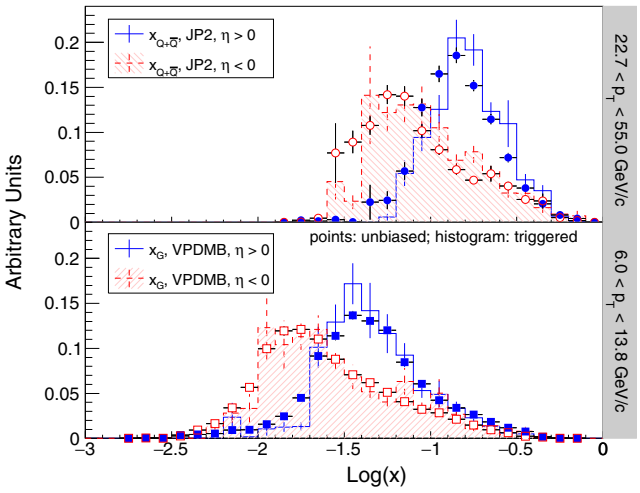

FIG. 6. Underlying parton x distribution for all Monte Carlo simulated jets (points) within the specified range of p_T compared to those passing the indicated event trigger condition (histogram). Uncertainties are from Monte Carlo statistics. The upper panel shows quark x values for high-p_T jets, comparing JP2 to unbiased events, while the bottom panel presents gluon x values for low-p_T jets, comparing VPDMB to unbiased events. For JP2, deviations can arise both from reconstruction effects and from bias in the event trigger. For VPDMB events, deviations from the unbiased sample arise from reconstruction and pileup effects.

E. Azimuthal resolutions

Since the asymmetries of interest are extracted from the azimuthal dependence of the spin-dependent cross sections, finite azimuthal resolution leads to a systematic dilution of the true asymmetries. There are two main contributors to the finite resolution: inefficiencies in TPC tracks and calorimeter towers, which distort the reconstruction of the jet thrust axis, and errors in the reconstructed positions of the tracks and towers. An additional resolution effect, finite azimuthal bin width, is discussed in Sec. III F. The size of the asymmetry smearing is estimated by evaluating the distribution of event-by-event deviations of the reconstructed azimuthal angles from their true value in the embedded simulation. The resulting distribution is convolved with a sinusoid, and the ratio of the resulting amplitude to the original is taken as the size of the dilution due to finite azimuthal resolution. This dilution is used to correct the measured asymmetries. Uncertainties for the resolution correction include both statistical contributions (from finite Monte Carlo statistics) and systematic contributions (e.g. from the accuracy of the Monte Carlo simulations).

The root mean square of the distribution of event-by-event jet-axis deviations is ~0.4 radians at the lowest jet p_T values and decreases to ~0.15 radians at high jet p_T. For inclusive-jet observables, this translates to finite azimuthal resolution effects of less than 10%. In low-p_T Collins and Collins-like asymmetries, smearing effects can become more significant. Enhanced smearing of the jet axis at low p_T due to less-collimated jets is compounded by the azimuthal resolution of the pion orientation. This carries with it a potentially strong dependence upon the proximity of the pion to the jet axis, denoted here as ΔR [Eq. (3)]. To ensure robust reconstruction of the relevant angles, a minimum cut on ΔR is imposed for the Collins and Collins-like asymmetries. The cut is optimized by balancing the degradation in azimuthal resolution with the loss in statistics. Furthermore, z and j_T become tightly correlated for more restrictive ΔR cuts. This is of crucial importance to the Collins asymmetry measurement which may have strong dependence upon both z and j_T. Specifically, the minimum j_T may be approximated

$$j_{T,\mathrm{min}} \approx z \times \Delta R_{\mathrm{min}} \times p_{T,\mathrm{jet}}, \tag{7}$$

where ΔR_{min} is the minimum ΔR, and $p_{T,\mathrm{jet}}$ is the p_T of the jet. Thus, the ΔR cut introduces a more stringent limit on j_T at higher values of jet p_T, where the present data are expected to have the most sensitivity to the Collins effect. For the analysis, $\Delta R_{\mathrm{min}} = 0.04$ is chosen. The resulting root mean square of the distribution of event-by-event ϕ_H deviations is ~0.78 radians at the lowest jet p_T values and decreases to ~0.40 radians at high jet p_T.

F. Nonuniform acceptance effects

The jet and pion yields for the various spin states depend upon all of the possible azimuthal modulations [17,43]. Twist-3 distributions (and indirectly the Sivers function) can give rise to modulations of the form $\sin(\phi_S)$. Transversity coupled to the polarized Collins fragmentation function can give rise to modulations of the form $\sin(\phi_S - \phi_H)$. Gluon linear polarization coupled to the polarized Collins-like fragmentation function can give rise to modulations of the form $\sin(\phi_S - 2\phi_H)$. In principle, modulations of the form $\sin(\phi_S + \phi_H)$ and $\sin(\phi_S + 2\phi_H)$ are also possible; but with the kinematic range of the present analysis they are expected to be negligible, even under maximized, positivity-bound scenarios [43]. Therefore, the corrections and systematic contributions are neglected in the present analysis for the latter two modulations. Nevertheless, their raw modulations have been examined and are found to be consistent with zero, and any corresponding systematic effect could constitute no more than 10%–20% of the total systematic uncertainty. In the limit of uniform acceptance, the cross ratios described in Sec. II F will isolate the desired observables, decoupled from the competing asymmetry modulations. The STAR detector has excellent uniformity. Nonetheless, small distortions in the detector response can couple to nonzero competing physics asymmetries to distort the extraction of the modulation of interest. These "leak-through" effects can manifest as a sinusoidal dependence in the angular distribution of interest or as higher-order Fourier components, depending on the combination of observables and level of nonuniform instrumental acceptance.

The shape of the leak-through distortion is extracted from the data, using a technique motivated by the conventional mixed-event procedure that is frequently used to measure acceptance effects. As an example, consider the distortion to the Collins modulation, $\phi_S - \phi_H$, due to the inclusive-jet asymmetry. Yields are binned for each event, in the same manner as with the asymmetry analysis. Events are given weights of

$$w_0 = 1 + A_{\mathrm{in}} \sin(\phi_S), \tag{8}$$

$$w_1 = 1 - A_{\mathrm{in}} \sin(\phi_S), \tag{9}$$

where A_{in} is an input asymmetry. Each event is binned twice, once for each proton spin state. The histogram corresponding to the actual spin state for the event is filled using weights of w_0, while the histogram for the opposite spin state is filled using weights of w_1. In this manner, an unpolarized sample is constructed (in the limit of vanishing luminosity asymmetries) removing the possibility for complications from actual physics coupling to the input asymmetries. A similar procedure is applied for each of the desired physics effects and their possible contaminations. The cross ratios for the relevant asymmetries are calculated using the weighted-event histograms and are fit with a function of the form

$$\epsilon(\phi) = p_0 + p_1 \sin(\phi) \tag{10}$$

(Sec. II F). The relevant distortions to the asymmetries of interest materialize in the p_1 parameter of the fit. A conservative systematic uncertainty due to finite acceptance effects is estimated as

$$\sigma_{\text{leak}} = \text{Max}(|A_{\text{leak}}|, \sigma_{A_{\text{leak}}}) \times \frac{\text{Max}(|p_1|, \sigma_{p_1})}{A_{\text{in}}}, \quad (11)$$

where A_{leak} is the measured asymmetry for the "competing" effect and A_{in} is the asymmetry weighted into the data for the study. For each of the asymmetries of interest, the leak-through systematic is calculated for each of the competing effects, and then added in quadrature to find the total systematic.

Distortions to the inclusive-jet asymmetry are found to be negligible. Distortions due to the Collins effect are reduced by the fact that π^+ and π^- asymmetries contribute with different signs and similar magnitudes. For the distortion due to the Collins-like effect, the asymmetries are modeled to have the same sign and magnitude for different pion states; however, the instrumental asymmetries are quite small, greatly suppressing the amount of possible distortion.

For the distortions to the Collins asymmetry, in particular due to the Collins-like asymmetry, the shapes are often quite far from sinusoidal. However, it is the sinusoidal modulations that determine the distortions, and these were found to be small in magnitude. Significant distortions of this kind should also manifest as highly degraded χ^2 distributions for the asymmetry extractions. As discussed in Sec. II F, the distributions are universally well behaved, indicating that the present data are not sensitive to such distortions. Finally, the gluon-based Collins-like effect should be significant only at low p_T, whereas the quark-based Collins effect should be significant only at high p_T. Consequently, no matter the size of the distortion from acceptance, the final distortions will be highly suppressed by the small size of the competing asymmetries. Accordingly, the only possible large distortions would arise from leak-through of the inclusive-jet asymmetry to the Collins-like asymmetry at low p_T, and vice versa. These distortions are highly suppressed by the relatively uniform acceptance.

A final acceptance-related systematic uncertainty is dilution from finite azimuthal bin width. The asymmetry is extracted by fitting the ϕ dependence of the cross ratios. The inclusive jet asymmetries are extracted using six azimuthal bins, while the Collins and Collins-like asymmetries are extracted using 12 azimuthal bins. The finite size of the bins will introduce a dilution to the extracted asymmetry, possibly further complicated by acceptance nonuniformity within the bins. The size of this effect can be calculated using the infrastructure developed for the leak-through estimates. Instead of weighting events with input asymmetries for the competing effects, events are weighted with input asymmetries for the desired effect. By fitting the resulting asymmetries, the extracted amplitude gives a precise estimate of the dilution from finite binning. The extracted value of the dilution (on the order of 1.5%) is consistent with what is expected for the size of the bins. These dilution values are used as a correction to the measured asymmetries.

G. Nonpion background

The backgrounds of main concern for inclusive jets are those events at the detector-jet level that do not associate with a parton jet (Sec. III C). For pions within jets, misidentified protons, kaons, and electrons represent an additional background. To estimate this contamination, data distributions of $n_\sigma(\pi)$ from the TPC (Sec. II E) and m^2 from TOF [61] are analyzed. Signal fractions are extracted by fitting m^2 with a multi-Voigt profile and $n_\sigma(\pi)$ with a multi-Gaussian function to extract yields for pions, kaons, protons, and electrons over the active ranges. Examples of these fits are shown in Figs. 7 and 8. The $n_\sigma(\pi)$ fits utilize corrections to the Bichsel theoretical dE/dx expectations similar to what is described in Ref. [61]. For each kinematic bin, the m^2 fits are performed for three different ranges of $n_\sigma(\pi)$, the values of which are varied according to the kinematics to create "pion-rich," "kaon-rich," and "proton-rich" samples. The shapes of the Voigt profiles are constrained to be independent of $n_\sigma(\pi)$, while the overall scales are allowed to vary.

Kaons and pions with a total momentum of 1.1 GeV/c experience the same dE/dx in the STAR TPC (see, e.g., Fig. 7), and protons and pions have the same dE/dx at a total momentum of 1.7 GeV/c. The multi-Gaussian $n_\sigma(\pi)$ fits are insufficient to determine the nonpion backgrounds in the vicinity of these crossovers. For bins of jet p_T and pion z corresponding to pion momenta below ~2.1 GeV/c, the TOF m^2 distributions (e.g. Fig. 7) are used exclusively to extract the pion, kaon, and proton fractions. For bins corresponding to pion momenta from ~2.1–3.5 GeV/c, the pion dE/dx values are well separated from those of kaons and protons. However, kaons and protons experience the same dE/dx at these kinematics in the STAR TPC. The m^2 resolution of the STAR TOF is not sufficient to separate pions from kaons at these momenta. Thus, a hybrid approach is used. The $n_\sigma(\pi)$ fits are used to extract the pion fractions and combined kaon and proton fractions. The isolated proton fractions are extracted from the m^2 distributions, where they are still well separated from pions and kaons. The kaon fractions are then taken from the difference between the combined $n_\sigma(\pi)$ kaon plus proton fractions and the m^2 proton fractions. For momenta above ~3.5 GeV/c, pion, kaon, and proton fractions are extracted exclusively from $n_\sigma(\pi)$ fits (e.g. Fig. 8). For all kinematics, electron fractions are determined from $n_\sigma(\pi)$ fits. In the kinematic regions where the kaon and proton dE/dx values

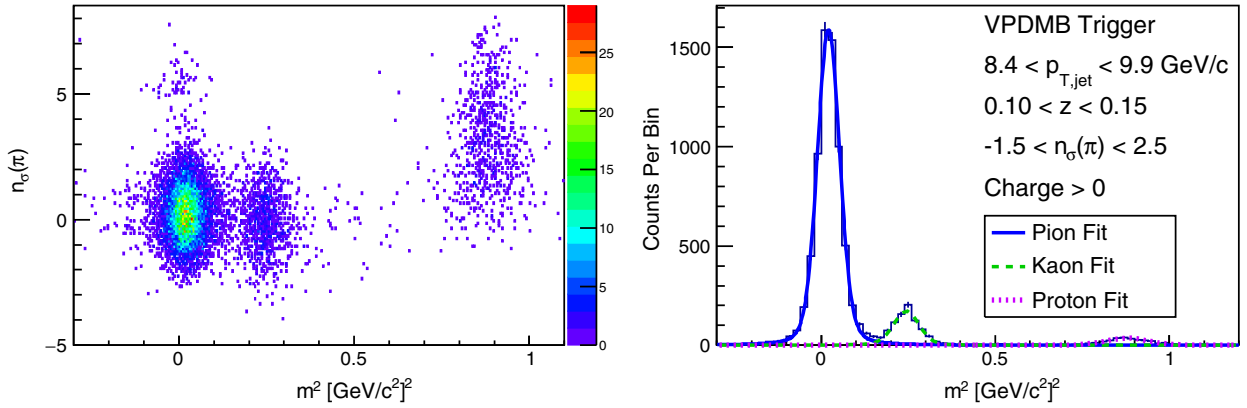

FIG. 7. $n_\sigma(\pi)$ vs m^2 (left) and a multi-Voigt-profile fit to m^2 (right) for VPDMB-triggered events with positively charged particles carrying momentum fractions of $0.10 < z < 0.15$ from jets with $8.4 < p_T < 9.9$ GeV/c. For the example fit shown, the charged particles are required to satisfy $-1.5 < n_\sigma(\pi) < 2.5$. The individual contributions to the overall fit from pions, kaons, and protons are shown.

are similar to those for pions, the kaons and protons contribute a ~10% background. Outside of these kinematic regions, the kaon and proton backgrounds are typically in the range of 1%–2%. Electrons typically contribute 1% or less.

The extracted pion, kaon, and proton fractions are used to correct the measured asymmetries. For each kinematic bin, asymmetries are measured for the three different ranges of $n_\sigma(\pi)$ discussed earlier. The corrected pion asymmetry is calculated as

$$A_\pi = \frac{A_1(f_2^K f_3^p - f_3^K f_2^p) + A_2(f_3^K f_1^p - f_1^K f_3^p) + A_3(f_1^K f_2^p - f_2^K f_1^p)}{f_1^\pi f_2^K f_3^p + f_2^\pi f_3^K f_1^p + f_3^\pi f_1^K f_2^p - f_1^\pi f_3^K f_2^p - f_2^\pi f_1^K f_3^p - f_3^\pi f_2^K f_1^p}. \tag{12}$$

Here, A_1, A_2, and A_3 are the asymmetries measured in the pion-rich, kaon-rich, and proton-rich $n_\sigma(\pi)$ ranges, respectively; f_1^π, f_1^K, and f_1^p are, respectively, the pion, kaon, and proton fractions from the pion-rich sample; f_2^π, f_2^K, and f_2^p are, respectively, the pion, kaon, and proton fractions from the kaon-rich sample; and f_3^π, f_3^K, and f_3^p are, respectively, the pion, kaon, and proton fractions from the proton-rich sample. Equation (12) assumes the electron asymmetry is negligible. The electron contamination is dominated by photonic electrons, largely from π^0 decay photons, and heavy flavor decays. Neutral pion asymmetries are expected to be approximately the averages of the π^+ and π^- asymmetries [45]. These averages are observed to be small in all cases, indicating the neutral pion asymmetries should also be small. Heavy flavor is produced primarily through gluon fusion for the present kinematic range. The $gg \to q\bar{q}$ process does not contribute to either the Collins or the Collins-like effect [72].

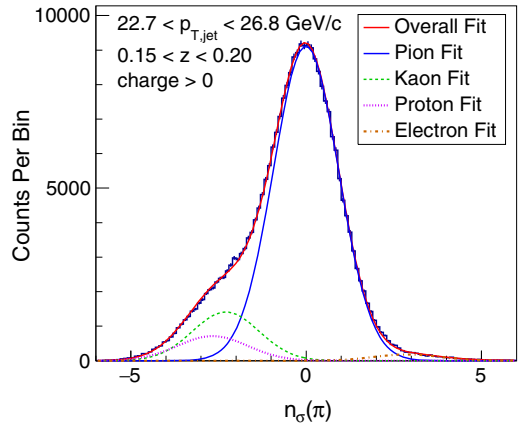

FIG. 8. Multi-Gaussian fit to the distribution of $n_\sigma(\pi)$ for positively charged particles from jets with $22.7 < p_T < 26.8$ GeV/c carrying momentum fractions of $0.15 < z < 0.20$. The overall fit is shown along with the individual portions for pions, kaons, protons, and electrons.

The systematic uncertainty for the correction is taken from the full differences between fractions extracted with different methodologies. For the momentum range below ~2.1 GeV/c, the uncertainties are the differences between fractions calculated from $n_\sigma(\pi)$ fits and m^2 fits. For momenta above ~2.1 GeV/c, the uncertainties are the differences between fractions from $n_\sigma(\pi)$ fits with and without fixing function parameters according to the corrected Bichsel expectations.

H. Polarization uncertainty

As mentioned in Sec. II A, a correlated systematic uncertainty of 3.5% applies to all single-spin asymmetries,

due to estimated uncertainties in the beam polarization [54]. This uncertainty includes a 3.3% contribution from the polarization scale, a 0.9% contribution from fill-to-fill scale uncertainties, and a 0.5% contribution from uncertainties in the transverse polarization profile correction. Additionally, if the beam polarization is not perfectly vertical with respect to the laboratory frame, there can also be a systematic uncertainty due to the horizontal or "radial" component of the beam polarization. For the present analysis, a polarization offset from vertical of δ will yield a dilution of approximately $1-\delta^2/2$, in the limit of uniform acceptance. The values for δ are measured by analyzing the azimuthal dependence of single-spin asymmetries in the ZDC, which is sensitive to neutral particles such as neutrons produced close to the beam line. The values for δ are generally quite small, typically $\ll 0.1$ rad [73]. Deviations due to nonuniform acceptance must, then, dominate. Conservatively, it is estimated that radial polarizations cannot impact the asymmetry extraction by more than fractions of a percent; and they are therefore ignored.

IV. RESULTS

Final results for the inclusive-jet, Collins, and Collins-like asymmetries are presented in Figs. 9 through 13. In all plots, the statistical uncertainties are shown with error bars, and systematic uncertainties are shown with shaded error boxes. The widths of the boxes indicate the total uncertainties in the kinematic variables that are corrected to the PYTHIA particle-jet level, as discussed in Sec. III B. For all results, the jet pseudorapidity is calculated relative to the polarized beam. In the cases of Collins and Collins-like asymmetries, π^+ is shown with closed circles, π^- with open circles, and the combination in closed diamonds. The 3.5% vertical-scale systematic uncertainties from beam polarization are not shown.

A. Inclusive jet asymmetry

In Fig. 9 the inclusive jet asymmetries are presented. The asymmetries are shown as functions of the jet transverse momentum and presented in separate ranges of jet pseudorapidity, as measured relative to the polarized beam. A dashed line at zero is provided to guide the eye. In all cases, the measured asymmetries are consistently small. Integrating over jet p_T and η the measured asymmetries are consistent with zero at the 0.5σ level with a total uncertainty of 6.0×10^{-4}. This is similar to what has been seen in previous inclusive jet measurements from $\sqrt{s}=200$ GeV collisions [48]. The present data at $\sqrt{s}=500$ GeV provide stronger limits with better sensitivity to gluonic subprocesses than previous data at $\sqrt{s}=200$ GeV [49]. Systematic uncertainties for the present data are well constrained, with the dominant uncertainties arising from statistics. The largest systematics arise from parton-jet matching probabilities at low values of p_T. At higher values of p_T, contributions from leak-through and trigger bias play a more significant role, though the effects are typically at or below 10% of the statistical uncertainty.

The inclusive-jet asymmetry is sensitive to the twist-3 distribution [15,16] related to the k_T-integrated Sivers function [19,23]. As the jet p_T increases, the sensitivity to partonic subprocesses changes (Fig. 3). At low jet p_T, the results are more sensitive to gluonic subprocesses, while sensitivity to quark-based subprocesses increases at high jet p_T. Thus the asymmetries at lower values of jet p_T should

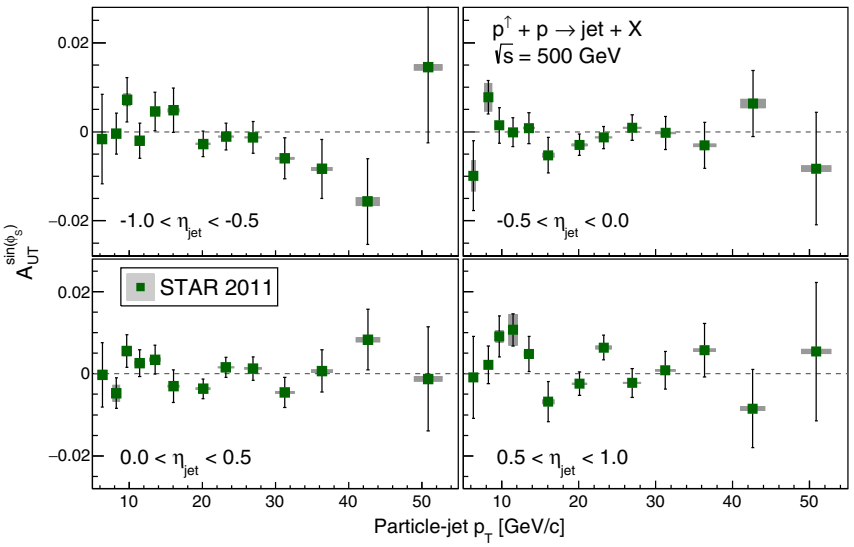

FIG. 9. Inclusive jet asymmetries $A_{UT}^{\sin(\phi_S)}$, also often referred to as A_N, as a function of particle-jet p_T. Statistical uncertainties are shown as error bars, while systematic uncertainties are shown as shaded error boxes. An additional 3.5% vertical scale uncertainty from polarization is correlated across all bins. Events are separated into different regions of jet η, calculated relative to the polarized beam. Across the full range of jet p_T, the measured asymmetries are consistently small.

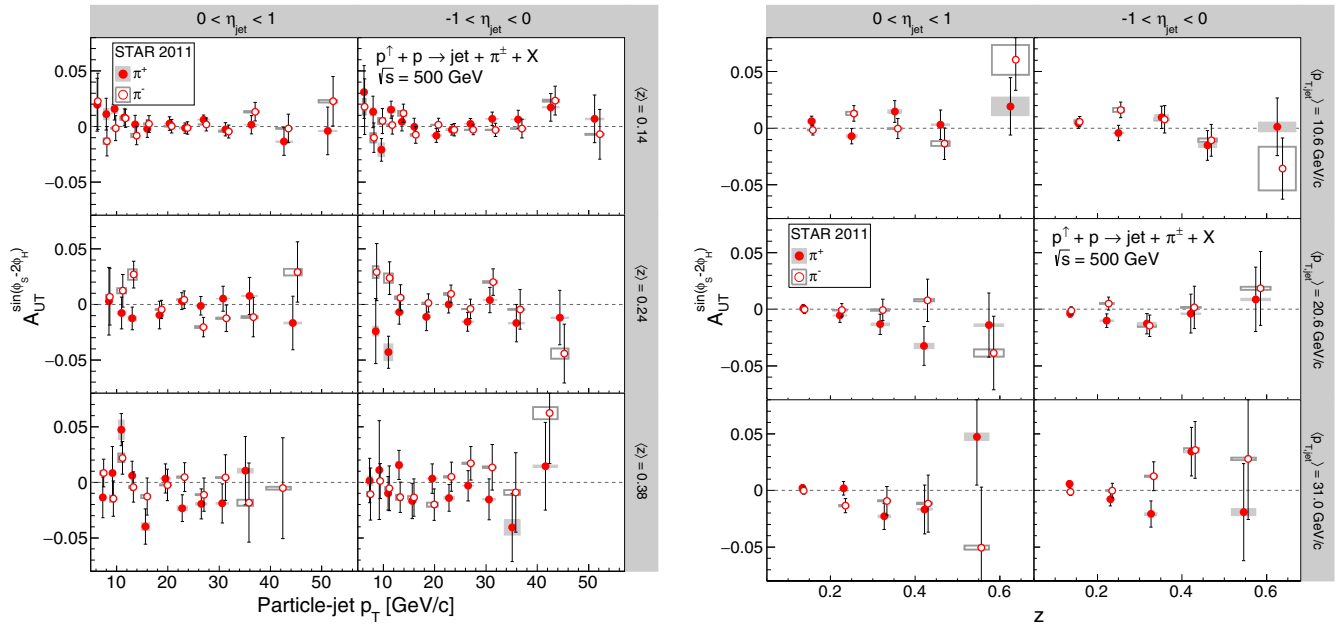

FIG. 10. Collins-like asymmetries as a function of particle-jet p_T (left) and as a function of pion z (right). π^- points are shifted horizontally for clarity. Statistical uncertainties are shown as error bars, while systematic uncertainties are shown as shaded error boxes. An additional 3.5% vertical scale uncertainty from polarization is correlated across all bins. Events are separated into different regions of jet η, calculated relative to the polarized beam. The jet p_T dependence is shown for three bins of pion z: $0.1 < z < 0.2$, $0.2 < z < 0.3$, and $0.3 < z < 0.8$. The pion z dependence is shown for three bins of jet p_T: $6.0 < p_T < 13.8$ GeV/c, $13.8 < p_T < 22.7$ GeV/c, and $22.7 < p_T < 55.0$ GeV/c. Asymmetries are consistently small.

place constraints on twist-3 PDFs for gluonic interactions (connected to the gluon Sivers function). As Fig. 6 indicates, the lowest jet p_T bins are sensitive to x_G down to ~0.01; while the highest bins probe x_Q up to ~0.2 for unpolarized x.

B. Collins-like asymmetry

Results for Collins-like asymmetries are presented in terms of particle-jet p_T and pion z (Figs. 10 and 11). Because the subprocess fraction changes as a function of particle-jet p_T, it is informative to examine how the asymmetries depend on p_T. The Collins-like asymmetry is expected to arise from gluon linear polarization [43]; thus, the best sensitivity should reside at lower values of jet p_T. The left-hand panel of Fig. 10 shows the asymmetry as a function of particle-jet p_T for different ranges of jet η and pion z. The right-hand panel of Fig. 10 presents the Collins-like asymmetry dependence on pion z in bins of jet η and jet p_T. Across the board, the asymmetries are consistently small. Systematic uncertainties are well constrained with

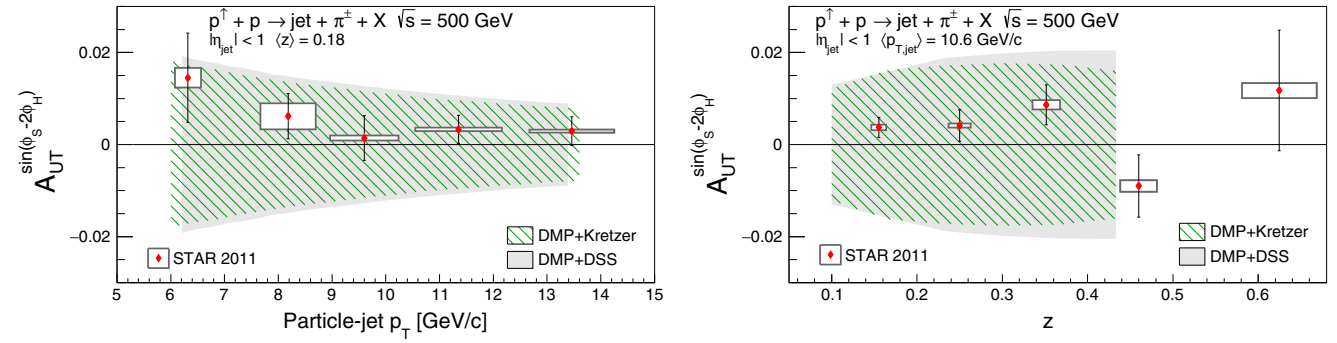

FIG. 11. Collins-like asymmetries as a function of particle-jet p_T for pions reconstructed with $0.1 < z < 0.3$ (left) and as a function of pion z for jets reconstructed with $6.0 < p_T < 13.8$ GeV/c (right). Asymmetries are shown combining π^+ and π^- and integrating over the full range of jet pseudorapidity, $-1 < \eta < 1$. Statistical uncertainties are shown as error bars, while systematic uncertainties are shown as shaded error boxes. An additional 3.5% vertical scale uncertainty from polarization is correlated across all bins. Shaded bands represent maximal predictions from Ref. [74] utilizing two sets of fragmentation functions [75,76]. The asymmetries are consistently small across the full range of jet p_T and pion z and provide the first experimental constraints on model calculations.

the dominant uncertainties arising from statistics. The largest systematics arise from the parton-jet matching probabilities at low-p_T and leak-through at mid-to-high values of p_T.

From Refs. [43,74], the maximized projections exhibit the largest asymmetries at lower values of both jet p_T and pion z. Furthermore, the maximized projections are similar for π^+ and π^- and for $\eta_{\rm jet} > 0$ and $\eta_{\rm jet} < 0$. Thus, in the left-hand panel of Fig. 11, the Collins-like asymmetries are presented as functions of jet p_T for $0.1 < z < 0.3$, combining pion flavors and integrating over the full range of $-1 < \eta_{\rm jet} < 1$. Similarly in the right-hand panel of Fig. 11, the asymmetries are presented as functions of pion z for jets with $6.0 < p_T < 13.8$ GeV/c, combining π^+ and π^- and integrating over the range $-1 < \eta_{\rm jet} < 1$. Again, systematic uncertainties are small, with the dominant uncertainties arising from statistics. The largest systematics arise from parton-jet matching probability at low p_T.

The asymmetries in Fig. 11 are presented in comparison with the maximized projections from Ref. [74]. The DMP + Kretzer calculations utilize fragmentation functions from Ref. [75], while the DMP + DSS calculations utilize fragmentation functions from Ref. [76]. The data place significant constraints on the maximized projections for the Collins-like asymmetries, representing the first experimental input for this effect, which is sensitive to linearly polarized gluons.

C. Collins asymmetry

Results for Collins asymmetries are presented as functions of particle-jet p_T and pion z in Fig. 12 and pion j_T in Fig. 13. In contrast to the Collins-like effect, the Collins asymmetry is expected to arise from quark transversity [20]; thus, the best sensitivity should reside at higher values of jet p_T. In the left-hand panel of Fig. 12 the asymmetry is presented as a function of particle-jet p_T for different ranges of jet η and pion z. A clear asymmetry is observed in jets with $p_T \gtrsim 20$ GeV/c and $\eta > 0$ relative to the polarized beam. While statistics are somewhat limited, the magnitude of the asymmetry also appears to rise from $0.1 < z < 0.2$ to $z > 0.2$. The observed asymmetries are positive for π^+ and negative for π^-. Global analyses from SIDIS and e^+e^- show positive u-quark transversity, negative d-quark transversity, positive favored Collins fragmentation functions, and negative unfavored Collins fragmentation functions. For the present kinematics, the preponderance of the π^+ and π^- are expected to materialize from the favored fragmentation of u and d quarks, respectively. Hence, the observed charge dependence is consistent with those of the Collins asymmetry in SIDIS [32,34,35] and marks the first such observation in polarized proton collisions. For pions with $0.1 < z < 0.2$ in jets with $p_T \gtrsim 20$ GeV/c and $\eta < 0$ relative to the polarized beam, there are also trends consistent with a nonzero asymmetry. However, these trends do not persist for higher values of

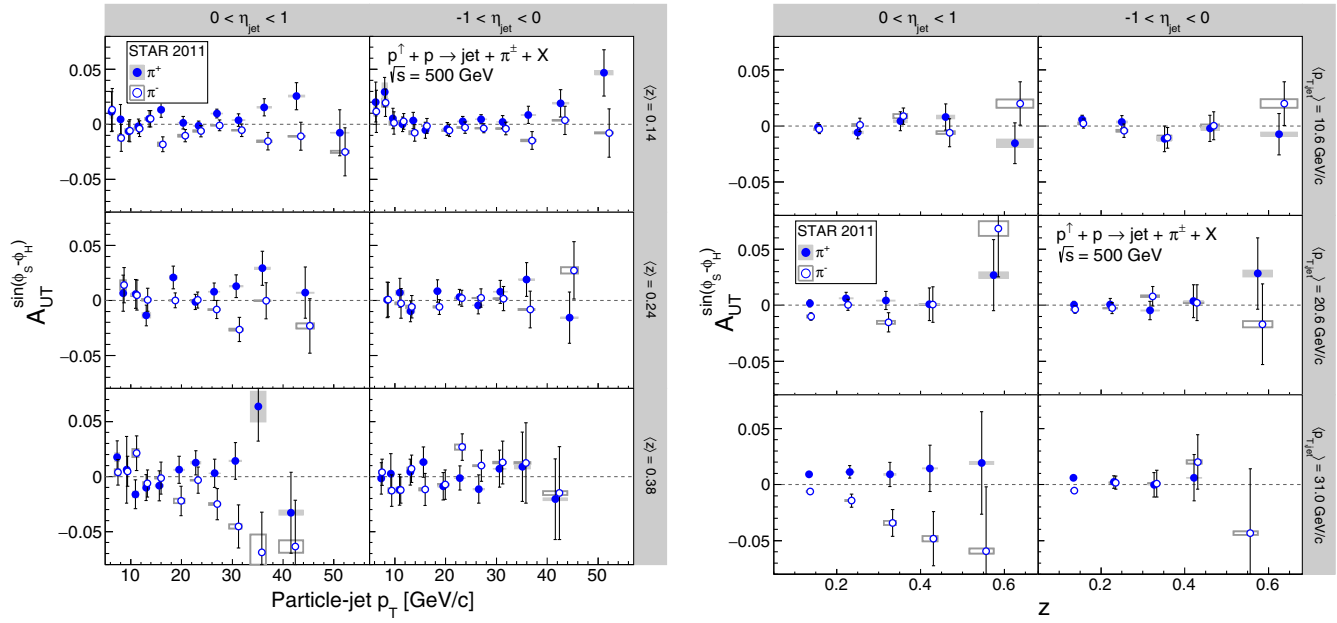

FIG. 12. Collins asymmetries as a function of particle-jet p_T (left) and as a function of pion z (right). π^- points are shifted horizontally for clarity. Asymmetries are shown separately for π^+ and π^- for two bins of jet η (relative to the polarized beam). The jet p_T dependence is presented in three bins of pion z: $0.1 < z < 0.2$, $0.2 < z < 0.3$, and $0.3 < z < 0.8$. The pion z dependence is presented in three bins of jet p_T: $6.0 < p_T < 13.8$ GeV/c, $13.8 < p_T < 22.7$ GeV/c, and $22.7 < p_T < 55.0$ GeV/c. Statistical uncertainties are shown as error bars, while systematic uncertainties are shown as shaded error boxes. An additional 3.5% vertical scale uncertainty from polarization is correlated across all bins. The asymmetry is observed to be nonzero for higher values of jet p_T and is the first such observation in polarized proton collisions.

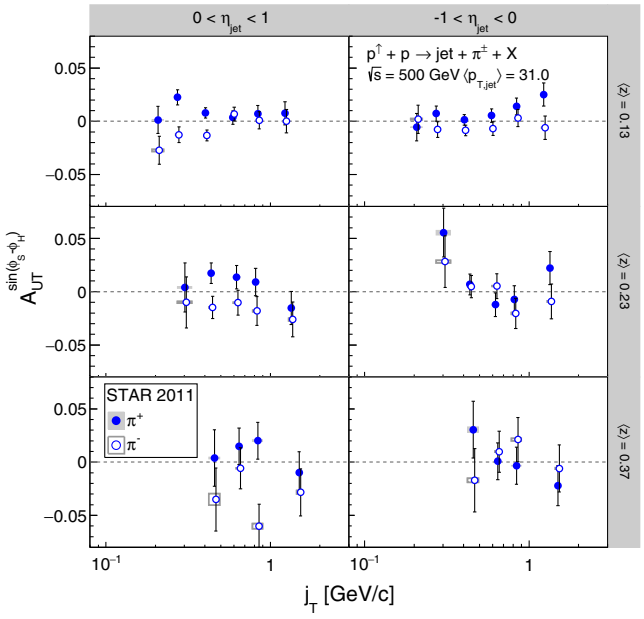

FIG. 13. Collins asymmetries as a function of pion j_T for jets reconstructed with $22.7 < p_T < 55.0$ GeV/c. Asymmetries are shown separately for π^+ and π^- for two bins of jet η (relative to the polarized beam) and three bins of pion z: $0.1 < z < 0.2$, $0.2 < z < 0.3$, and $0.3 < z < 0.8$. Statistical uncertainties are shown as error bars, while systematic uncertainties are shown as shaded error boxes. An additional 3.5% vertical scale uncertainty from polarization is correlated across all bins. Asymmetries appear to show a dependence upon j_T with the largest effects at the lower j_T values.

pion z; and thus it is not clear if this effect is due to physics or simply a statistical fluctuation.

The right-hand panel of Fig. 12 presents the Collins asymmetries as functions of pion z for three bins of jet p_T and two bins of jet η, calculated relative to the polarized beam. The magnitude of the Collins asymmetry is expected to change as a function of z [36]. At high p_T the present data indicate asymmetries with such a dependence. For jets scattered backward relative to the polarized beam, as well as for jets with lower values of p_T, the measured asymmetries are small. This is also consistent with expectation for the Collins effect. As the p_T increases, the present data sample a correspondingly increasing fraction of events from quark-based partonic subprocesses (Fig. 3) that are necessary for such effects. Furthermore, the present data sample higher values of x with increasing values jet p_T. Current global extractions of transversity indicate a potentially strong x dependence [38–42]. Unpolarized Monte Carlo simulations indicate that for jets reconstructed with $22.7 < p_T < 55.0$ GeV/c, the sampled quark x range peaks around $x \sim 0.15$ (Fig. 6). This corresponds to the region where the largest values of transversity are expected [38–42] but with $Q^2 \approx 960$ GeV^2, significantly higher than the scale probed by the SIDIS data with $Q^2 < 20$ GeV^2.

For the present data, systematic uncertainties are small compared to the statistical uncertainties. As with the Collins-like asymmetries, the dominant systematics at low jet p_T arise from the parton-jet matching probabilities. At higher jet p_T values, the dominant sources of systematics arise from leak-through and trigger bias, though the systematic uncertainties are typically only ∼15% of the statistical uncertainties.

The Collins effect requires not only nonzero transversity but also the presence of a polarized and transverse-momentum-dependent fragmentation function. Thus, while it is informative to examine the jet p_T and pion z dependences of the Collins effect, it is also important to examine its j_T dependence. This study examines how the asymmetry depends upon the relative transverse momentum of the pion, in other words, the pion momentum transverse to the jet axis. The results for the present data are presented in Fig. 13 for jets with $22.7 < p_T < 55.0$ GeV/c in three bins of pion z. The asymmetries appear largest around $j_T \sim 0.3$–0.4 GeV/c. It is worth noting, again, that the choice of a lower limit on ΔR restricts the lower reach of j_T, in particular at higher values of pion z or jet p_T [Eq. (7)].

Integrating over all bins of z at high jet p_T, the present Collins asymmetries for π^+ and π^- are found to be different with a significance of greater than 5.3σ. Consequently, the present data represent the first observation of the Collins effect in polarized-proton collisions.

D. Comparison to models

The present data span a range of quark x which complements existing SIDIS measurements and current transversity extractions [38–42] but at 1–2 orders of magnitude higher in Q^2, as seen in Fig. 2. Accordingly, the present data present an opportunity to address existing theoretical questions concerning universality and the size of possible TMD factorization-breaking effects in polarized-proton collisions, and TMD evolution.

Figure 14 presents the Collins asymmetries for jets reconstructed with $22.7 < p_T < 55.0$ GeV/c and $0 < \eta < 1$ in comparison with three sets of model calculations. Each set is based upon a global analysis of SIDIS and e^+e^- data, assumes robust TMD factorization applied to proton-proton interactions, and assumes universality of the Collins fragmentation function. The DMP + 2013 predictions are based upon Refs. [40,43,74] and utilize the fragmentation functions from Ref. [76]. Reference [74] also presents predictions based upon older models from Refs. [38,39]. These older predictions demonstrate that the size of the expected asymmetries can be sensitive to the choice of fragmentation functions, in particular for the $g \to \pi^{\pm}$ contribution that still has considerable uncertainty [77]. The Kang-Prokudin-Ringer-Yuan (KPRY) and KPRY-NLL predictions are based upon Ref. [78]. The KPRY-NLL curves assume TMD evolution up to next-to-leading log, while the KPRY curves assume no TMD evolution. In general the models compare

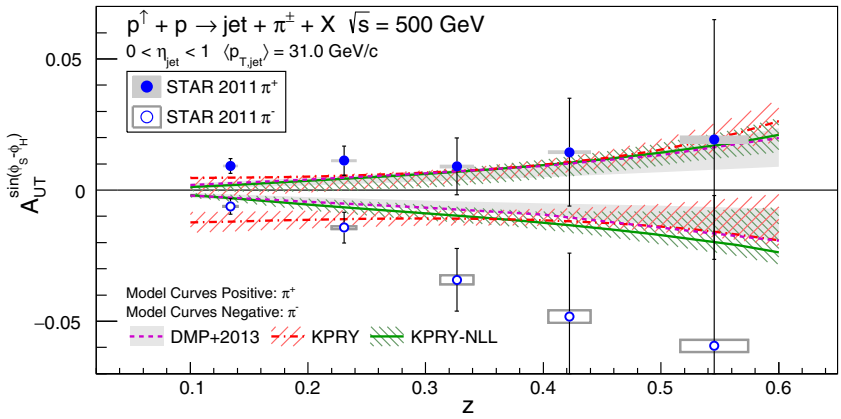

FIG. 14. Collins asymmetries as a function of pion z for jets reconstructed with $22.7 < p_T < 55.0$ GeV/c and $0 < \eta < 1$. The asymmetries are shown in comparison with model calculations from Refs. [74,78]. The calculations are based upon SIDIS and e^+e^- results and assume robust factorization and universality of the Collins function. The DMP + 2013 [74] and KPRY [78] predictions assume no TMD evolution, while the KPRY-NLL [78] curves assume TMD evolution up to next-to-leading log. All predictions are shown with shaded bands corresponding to the size of their associated theoretical uncertainties. The general agreement between the data and the model calculations is consistent with assumptions of robust TMD factorization and universality of the Collins function.

favorably with the data, consistent with the expectation of universality of the Collins fragmentation function. In addition, this comparison is also consistent with the assumption of robust TMD factorization for proton-proton interactions. While it is generally expected that TMD factorization is broken for proton-proton interactions, it has been argued that such factorization holds for observation of a hadron fragment within a jet [29,45]. Within theoretical uncertainties, the data agree relatively well with either assumption of TMD evolution from the KPRY predictions. However, the data do show a slight preference for the model without TMD evolution ($\chi^2 = 14.0$ for 10 degrees of freedom without evolution compared with $\chi^2 = 17.6$ with evolution, using the data statistical and systematic uncertainties). The measured asymmetries are generally larger in magnitude than the model predictions, in particular for π^-. A χ^2 test indicates the measurement and predictions are consistent at the 95% confidence level.

Finally, it is worth noting that polarized-proton collisions at STAR have also yielded nonzero asymmetries sensitive to transversity through dihadron interference fragmentation functions [79]. These asymmetries persist in the collinear framework of pQCD, where factorization and universality are expected to hold [80]. Efforts to include these results in global analyses aimed at extracting transversity have already begun [81]. The combination of the present results with those from e^+e^-, SIDIS, and dihadrons from $p + p$ provides the opportunity for a comprehensive global analysis to address questions concerning TMD-factorization breaking, universality, and evolution.

V. CONCLUSIONS

We have reported the first measurements of transverse single-spin asymmetries from inclusive jet and jet + $\pi^{\pm}$ production in the central pseudorapidity range from $p^{\uparrow} + p$ at $\sqrt{s} = 500$ GeV. The data were collected in 2011 with the STAR detector. As in previous measurements at 200 GeV, the inclusive jet asymmetry is consistent with zero at the available precision. The first-ever measurements of the "Collins-like" asymmetry, sensitive to linearly polarized gluons in a polarized proton, are found to be small and provide the first constraints on model calculations. For the first time, we observe a nonzero Collins asymmetry in polarized-proton collisions. The data probe values of Q^2 significantly higher than existing measurements from SIDIS. The asymmetries exhibit a dependence on pion z and are consistent in magnitude for the two charged-pion species. For π^+, asymmetries are found to be positive, while those for π^- are found to be negative. The present data are compared to Collins asymmetry predictions based upon SIDIS and e^+e^- data. The comparisons are consistent with the expectation for TMD factorization in proton-proton collisions and universality of the Collins fragmentation function. The data show a slight preference for models assuming no suppression from TMD evolution. Further insight into these theoretical questions can be gained from a global analysis, including dihadron asymmetries and Collins asymmetries from STAR.

ACKNOWLEDGMENTS

The authors thank Zhong-Bo Kang, Alexei Prokudin, Umberto D'Alesio, and Cristian Pisano for valuable discussions and providing the results of their model calculations. We thank the RHIC Operations Group and RCF at BNL, the NERSC Center at LBNL, and the Open Science Grid consortium for providing resources and support. This work was supported in part by the Office of Nuclear Physics within the U.S. DOE Office of Science,

the U.S. National Science Foundation, the Ministry of Education and Science of the Russian Federation, National Natural Science Foundation of China, Chinese Academy of Science, the Ministry of Science and Technology of China and the Chinese Ministry of Education, the National Research Foundation of Korea, GA, and MSMT of the Czech Republic, Department of Atomic Energy and Department of Science and Technology of the Government of India, the National Science Centre of Poland, National Research Foundation, the Ministry of Science, Education and Sports of the Republic of Croatia, RosAtom of Russia and German Bundesministerium fur Bildung, Wissenschaft, Forschung and Technologie (BMBF) and the Helmholtz Association.

[1] J. Ralston and D. Soper, Nucl. Phys. **B152**, 109 (1979); R. L. Jaffe and X. Ji, Phys. Rev. Lett. **67**, 552 (1991).
[2] F. D. Aaron *et al.* (H1 and ZEUS Collaborations), J. High Energy Phys. 01 (2010) 109.
[3] D. de Florian, R. Sassot, M. Stratmann, and W. Vogelsang, Phys. Rev. Lett. **101**, 072001 (2008); Phys. Rev. D **80**, 034030 (2009); Phys. Rev. Lett. **113**, 012001 (2014).
[4] J. Blümlein and H. Böttcher, Nucl. Phys. **B841**, 205 (2010).
[5] E. Leader, A. V. Sidorov, and D. B. Stamenov, Phys. Rev. D **82**, 114018 (2010).
[6] R. D. Ball, S. Forte, A. Guffanti, E. R. Nocera, G. Ridolfi, and J. Rojo (NNPDF Collaboration), Nucl. Phys. **B874**, 36 (2013); E. R. Nocera, R. D. Ball, S. Forte, G. Ridolfi, and J. Rojo (NNPDF Collaboration), *ibid.* **B887**, 276 (2014).
[7] G. L. Kane, J. Pumplin, and W. Repko, Phys. Rev. Lett. **41**, 1689 (1978).
[8] W. Dragoset, J. B. Roberts, J. E. Bowers, H. W. Courant, H. Kagan, M. L. Marshak, E. A. Peterson, K. Ruddick, and R. D. Klem, Phys. Rev. D **18**, 3939 (1978).
[9] J. Antille, L. Dick, L. Madansky, D. Perret-Gallix, M. Werlen, A. Gonidec, K. Kuroda, and P. Kyberd, Phys. Lett. **94B**, 523 (1980).
[10] B. E. Bonner *et al.* (FNAL-E704 Collaboration), Phys. Rev. Lett. **61**, 1918 (1988); D. L. Adams *et al.* (FNAL E581/704 Collaboration), Phys. Lett. B **261**, 201 (1991); D. L. Adams *et al.* (FNAL E704 Collaboration), *ibid.* **264**, 462 (1991); A. Bravar *et al.* (Fermilab E704 Collaboration), Phys. Rev. Lett. **77**, 2626 (1996).
[11] S. Sarof *et al.*, Phys. Rev. Lett. **64**, 995 (1990).
[12] J. Adams *et al.* (STAR Collaboration), Phys. Rev. Lett. **92**, 171801 (2004); B. I. Abelev *et al.* (STAR Collaboration), *ibid.* **101**, 222001 (2008); L. Adamczyk *et al.* (STAR Collaboration), Phys. Rev. D **86**, 051101(R) (2012).
[13] I. Arsene *et al.* (BRAHMS Collaboration), Phys. Rev. Lett. **101**, 042001 (2008).
[14] A. Adare *et al.* (PHENIX Collaboration), Phys. Rev. D **90**, 012006 (2014).
[15] A. Efremov and O. Teryaev, Yad. Fiz. **36**, 242 (1982) [Sov. J. Nucl. Phys. **36**, 140 (1982)].
[16] J. Qiu and G. Sterman, Phys. Rev. D **59**, 014004 (1998).
[17] K. Kanazawa and Y. Koike, Phys. Lett. B **720**, 161 (2013).
[18] K. Kanazawa, Y. Koike, A. Metz, and D. Pitonyak, Phys. Rev. D **89**, 111501(R) (2014).
[19] D. Sivers, Phys. Rev. D **41**, 83 (1990); **43**, 261 (1991).
[20] J. Collins, Nucl. Phys. **B396**, 161 (1993).
[21] S. J. Brodsky, D. S. Hwang, and I. Schmidt, Phys. Lett. B **530**, 99 (2002).
[22] J. C. Collins, Phys. Lett. B **536**, 43 (2002).
[23] D. Boer, P. J. Mulders, and F. Pijlman, Nucl. Phys. **B667**, 201 (2003).
[24] X.-d. Ji, J.-P. Ma, and F. Yuan, Phys. Lett. B **597**, 299 (2004); Phys. Rev. D **71**, 034005 (2005).
[25] J. C. Collins and A. Metz, Phys. Rev. Lett. **93**, 252001 (2004).
[26] Z.-B. Kang and J.-W. Qiu, Phys. Rev. Lett. **103**, 172001 (2009).
[27] J. Collins and J.-W. Qiu, Phys. Rev. D **75**, 114014 (2007); J. Collins, arXiv:0708.4410.
[28] T. C. Rogers and P. J. Mulders, Phys. Rev. D **81**, 094006 (2010).
[29] Z.-B. Kang, X. Liu, F. Ringer, and H. Xing, J. High Energy Phys. 11 (2017) 068.
[30] X. Ji, J. W. Qiu, W. Vogelsang, and F. Yuan, Phys. Rev. Lett. **97**, 082002 (2006); Phys. Rev. D **73**, 094017 (2006); Phys. Lett. B **638**, 178 (2006).
[31] L. Gamberg, Z.-B. Kang, and A. Prokudin, Phys. Rev. Lett. **110**, 232301 (2013).
[32] A. Airapetian *et al.* (HERMES Collaboration), Phys. Rev. Lett. **94**, 012002 (2005); Phys. Lett. B **693**, 11 (2010).
[33] A. Airapetian *et al.* (HERMES Collaboration), Phys. Rev. Lett. **103**, 152002 (2009).
[34] V. Y. Alexakhin *et al.* (COMPASS Collaboration), Phys. Rev. Lett. **94**, 202002 (2005); E. S. Ageev *et al.* (COMPASS Collaboration), Nucl. Phys. **B765**, 31 (2007); M. G. Alekseev *et al.* (COMPASS Collaboration), Phys. Lett. B **673**, 127 (2009); **692**, 240 (2010); C. Adolph *et al.* (COMPASS Collaboration), *ibid.* **717**, 376 (2012); **744**, 250 (2015).
[35] X. Qian *et al.* (Jefferson Lab Hall A Collaboration), Phys. Rev. Lett. **107**, 072003 (2011).
[36] R. Seidl *et al.* (Belle Collaboration), Phys. Rev. Lett. **96**, 232002 (2006); Phys. Rev. D **86**, 039905(E) (2012).
[37] J. P. Lees *et al.* (*BABAR* Collaboration), Phys. Rev. D **90**, 052003 (2014).
[38] M. Anselmino, M. Boglione, U. D'Alesio, A. Kotzinian, F. Murgia, A. Prokudin, and C. Turk, Phys. Rev. D **75**, 054032 (2007).
[39] M. Anselmino, M. Boglione, U. D'Alesio, F. Kotzinian, S. Melis, F. Murgia, and A. Prokudin, Nucl. Phys. B, Proc. Suppl. **191**, 98 (2009).

[40] M. Anselmino, M. Boglione, U. D'Alesio, S. Melis, F. Murgia, and A. Prokudin, Phys. Rev. D **87**, 094019 (2013).
[41] M. Anselmino, M. Boglione, U. D'Alesio, J. O. Gonzalez Hernandez, S. Melis, F. Murgia, and A. Prokudin, Phys. Rev. D **92**, 114023 (2015).
[42] Z.-B. Kang, A. Prokudin, P. Sun, and F. Yuan, Phys. Rev. D **93**, 014009 (2016).
[43] U. D'Alesio, F. Murgia, and C. Pisano, Phys. Rev. D **83**, 034021 (2011).
[44] M. Anselmino, M. Boglione, U. D'Alesio, E. Leader, S. Melis, and F. Murgia, Phys. Rev. D **73**, 014020 (2006).
[45] F. Yuan, Phys. Rev. Lett. **100**, 032003 (2008); Phys. Rev. D **77**, 074019 (2008).
[46] D. Boer and P. J. Mulders, Phys. Rev. D **57**, 5780 (1998).
[47] D. Boer, C. Lorcé, C. Pisano, and J. Zhou, Adv. High Energy Phys. **2015**, 371396 (2015).
[48] L. Adamczyk *et al.* (STAR Collaboration), Phys. Rev. D **86**, 032006 (2012).
[49] A. Mukherjee and W. Vogelsang, Phys. Rev. D **86**, 094009 (2012).
[50] H.-L. Lai, M. Guzzi, J. Huston, Z. Li, P. M. Nadolsky, J. Pumplin, and C.-P. Yuan, Phys. Rev. D **82**, 074024 (2010).
[51] M. Harrison, T. Ludlam, and S. Ozaki, Nucl. Instrum. Methods Phys. Res., Sect. A **499**, 235 (2003); H. Hahn *et al.*, *ibid.* **499**, 245 (2003).
[52] K. H. Ackermann *et al.* (STAR Collaboration), Nucl. Instrum. Methods Phys. Res., Sect. A **499**, 624 (2003).
[53] I. Alekseev *et al.*, Nucl. Instrum. Methods Phys. Res., Sect. A **499**, 392 (2003).
[54] RHIC Polarimetry Group, RHIC Polarizations for Runs 9-12, Report No. C-A/AP/490, 2013.
[55] O. Jinnouchi *et al.*, in *Proceedings of the 16th International Symposium on Spin Physics (Spin2004)* (World Scientific, Singapore, 2005).
[56] H. Okada *et al.*, Phys. Lett. B **638**, 450 (2006).
[57] F. S. Bieser *et al.*, Nucl. Instrum. Methods Phys. Res., Sect. A **499**, 766 (2003).
[58] W. J. Llope *et al.*, Nucl. Instrum. Methods Phys. Res., Sect. A **759**, 23 (2014).
[59] W. Anderson *et al.*, Nucl. Instrum. Methods Phys. Res., Sect. A **499**, 659 (2003).
[60] W. J. Llope, Nucl. Instrum. Methods Phys. Res., Sect. B **241**, 306 (2005).
[61] M. Shao, O. Barannikova, X. Dong, Y. Fisyak, L. Ruan, P. Sorensen, and Z. Xu, Nucl. Instrum. Methods Phys. Res., Sect. A **558**, 419 (2006); Y. Xu *et al.*, *ibid.* **614**, 28 (2010).
[62] M. Beddo *et al.*, Nucl. Instrum. Methods Phys. Res., Sect. A **499**, 725 (2003).
[63] C. E. Allgower *et al.*, Nucl. Instrum. Methods Phys. Res., Sect. A **499**, 740 (2003).
[64] S. Margetis and D. Cebra, STARNote SN0089 (1994); R. Reed, J. Balewski, L. S. Barnby, A. Ogawa, J. Lauret, and M. van Leeuwen, J. Phys. Conf. Ser. **219**, 032020 (2010).
[65] L. Adamczyk *et al.* (STAR Collaboration), Phys. Rev. Lett. **115**, 092002 (2015).
[66] M. Cacciari, G. P. Salam, and G. Soyez, J. High Energy Phys. 04 (2008) 063.
[67] M. Cacciari, G. P. Salam, and G. Soyez, Eur. Phys. J. C **72**, 1896 (2012).
[68] G. G. Ohlsen and P. W. Keaton, Nucl. Instrum. Methods **109**, 41 (1973).
[69] T. Sjöstrand, S. Mrenna, and P. Skands, J. High Energy Phys. 05 (2006) 026.
[70] P. Z. Skands, Phys. Rev. D **82**, 074018 (2010).
[71] R. Brun, F. Bruyant, M. Maire, A. C. McPherson, and P. Zanarini, GEANT3 Report No. CERN-DD-EE-84-1 (1987), http://inspirehep.net/record/252007; R. Brun, F. Bruyant, F. Carminati, S. Giani, M. Maire, A. McPherson, G. Patrick, and L. Urban, Reports No. CERN-W5013, No. CERN-W-5013, No. W5013, No. W-5013 (1994), http://inspirehep.net/record/863473.
[72] E. Leader, Camb. Monogr. Part. Phys. Nucl. Phys. Cosmol. **15**, 1 (2011).
[73] STAR ZDC Polarimetry Group, ZDC Scaler Polarimetry, http://online.star.bnl.gov/scaler2011/polarimetry/.
[74] U. D'Alesio, F. Murgia, and C. Pisano, Phys. Lett. B **773**, 300 (2017).
[75] S. Kretzer, Phys. Rev. D **62**, 054001 (2000).
[76] D. de Florian, R. Sassot, and M. Stratmann, Phys. Rev. D **75**, 114010 (2007).
[77] D. de Florian, R. Sassot, M. Epele, R. J. Hernández-Pinto, and M. Stratmann, Phys. Rev. D **91**, 014035 (2015).
[78] Z.-B. Kang, A. Prokudin, F. Ringer, and F. Yuan, Phys. Lett. B **774**, 635 (2017).
[79] L. Adamczyk *et al.* (STAR Collaboration), Phys. Rev. Lett. **115**, 242501 (2015); J. Adams *et al.* (STAR Collaboration), arXiv:1710.10215.
[80] A. Bacchetta and M. Radici, Phys. Rev. D **70**, 094032 (2004).
[81] M. Radici, Proc. Sci. DIS2017 (**297**) 229 (2018).